On persistent primary variables for numerical modeling of gas migration in a nuclear waste repository

Alain Bourgeat, Mladen Jurak & Farid Smaï

Computational Geosciences
Modeling, Simulation and Data Analysis

ISSN 1420-0597
Volume 17
Number 2

Comput Geosci (2013) 17:287-305
DOI 10.1007/s10596-012-9331-1

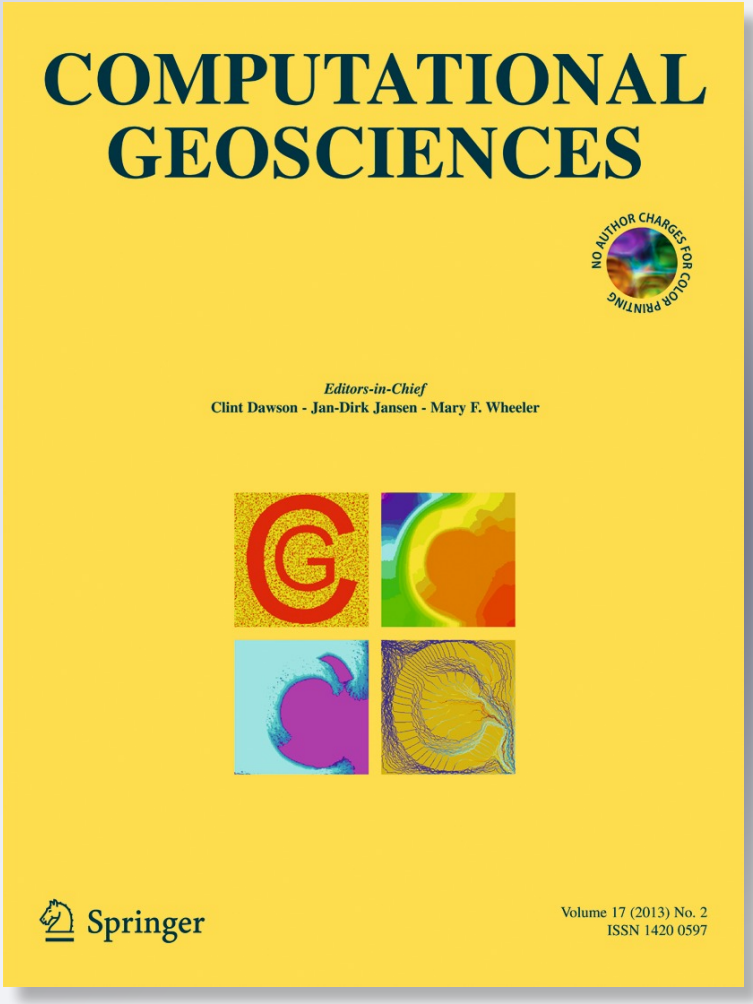

Springer

Comput Geosci (2013) 17:287–305
DOI 10.1007/s10596-012-9331-1

ORIGINAL PAPER

On persistent primary variables for numerical modeling of gas migration in a nuclear waste repository

Alain Bourgeat · Mladen Jurak · Farid Smaï

Received: 19 January 2012 / Accepted: 15 November 2012 / Published online: 21 December 2012

Abstract Numerical simulation of gas migration driven by compressible two-phase partially miscible flow in porous media is of major importance for safety assessment of deep geological repositories for long-lived high-level nuclear waste. We present modeling of compositional liquid and gas flow for numerical simulations of hydrogen migration in deep geological radioactive waste repository based on persistent primary variables. Two-phase flow is considered, with incompressible liquid and compressible gas, which includes capillary effects, gas dissolution, and diffusivity. After discussing briefly the existing approaches to deal with phase appearance and disappearance problem, including a persistent set of variables already considered in a previous paper (Bourgeat et al., Comput Geosci 13(1):29–42, 2009), we focus on a new variant of the primary variables: dissolved hydrogen mass concentration and liquid pressure. This choice leads to a unique and consistent formulation in liquid saturated and unsaturated regions, which is well adapted to heterogeneous media. We use this new set of variable for numerical simulations and show computational evidences of its adequacy to simulate gas phase appearance and disappearance in different but typical situations for gas migration in an underground radioactive waste repository.

Keywords Two-phase flow · Compositional flow · Porous medium · Underground nuclear waste management · Gas migration · Persistent primary variables

A. Bourgeat · F. Smaï
CNRS UMR 5208 Institut Camille Jordan,
Université de Lyon, Université Lyon 1,
69200 Villeurbanne, France

M. Jurak (✉)
Faculty of Science, University of Zagreb,
Bijenicka 30, Zagreb, Croatia
e-mail: jurak@math.hr

1 Introduction

The simultaneous flow of immiscible fluids in porous media occurs in a wide variety of applications. The most concentrated research in the field of multiphase flows over the past four decades has focused on unsaturated groundwater flows and flows in underground petroleum reservoirs. Most recently, multiphase flows have generated serious interest among engineers concerned with deep geological repository for radioactive waste and for CO_2 capture and storage simulations.

The low permeability argillites are considered in several European countries as possible host rock for the geological underground storage of radioactive wastes (see [3, 18, 29, 30, 34, 36, 37, 41]). The storage concepts are based on series of passive complementary barriers consisting both of engineered and natural materials, designed to isolate radionuclides contained in the waste and to slow down their release into the environment. These barriers compose a heterogeneous porous media highly saturated with water, but undergoing several resaturation–desaturation cycles during the transitory period of up to hundred thousand years following the excavation. Due to low porosity and permeability of the argillaceous host rock (COX for instance) and also

of some materials used for sealing tunnels (like bentonite), the desaturation is connected with appearance of strong capillarity effects that affect the flow patterns. Moreover, in the post-closure period, the excavation-induced desaturation is enhanced by the production of hydrogen from the anaerobic corrosion of steel engineered barriers (carbon steel overpacks and stainless steel casing). From stochiometric arguments, the amount of hydrogen generated by corrosion is expected to be sufficiently substantial and fast to produce a free gas phase which, due to relatively limited free volume available within the excavation, can lead to significant buildup pressure. In some studies, it has been found that the maximal pressure can exceed several megapascal and then perturb both the engineered barriers and the EDZ or even the host rock. Moreover, the gas phase dissipation is slowed down both by the low permeability of the host rock and the many bentonite seals along the excavation; such gas buildup pressure will then produce local gradients of hydraulic charge and perturb the process of seals' resaturation. There is even a growing awareness that the effect of hydrogen gas generation can affect all the functions allocated to the canisters, the buffers, and the backfill (see [18, 37, 41]) and even threaten, by overpressurization, the host rock safety function [8], fracturing the host rock and inducing groundwater flow and transport of radionuclides outside the waste site boundaries. Our ability to understand and predict underground gas migration within multimaterial porous system is a key component in the designing and the performance assessment of any reliable geological nuclear waste storage.

In nuclear waste management, the migration of gas through the near-field environment and the host rock involves two components, water and pure hydrogen H_2, and two phases: "liquid" and "gas." Due to the inherent complexity of the physics, equations governing this type of flow in porous media are nonlinear and coupled. Moreover, the geometries and material properties characterizing many applications can be quite irregular and contrasted. As a result of all these difficulties, numerical simulation often offers the only viable approach to modeling transport and multiphase flows in porous media.

An important consideration, in the modeling of fluid flow with mass exchange between phases, is the choice of the primary variables that define the thermodynamic state of the system. When a phase appears or disappears, the set of appropriate thermodynamic variables may change. There are two different approaches to that problem. The first one, widely used in simulators such as TOUGH2 [40], relies on a primary variable substitution algorithm. This algorithm uses in two-phase conditions the appropriate variables like pressure and saturation, and when a transition to single-phase conditions occurs, it switches to new variables adapted to the one-phase conditions, like pressure and concentration. This variable substitution is done after each Newton iteration according to some "switching criteria," see [13, 21, 38, 43]. A different presentation of this approach was done recently in [22, 24, 26], where the solubility conditions are formulated as complementary conditions which complement the conservation law equations. The whole system is then solved by a semi-smooth Newton method, first introduced in this context in [25], see also [16, 44], which consists in working on an intermediate active node set (see [26]). The second possibility is, like in [4, 9], to use a set of primary "persistent" variables, such as pressure and component density, which will remain well defined when phase conditions change, so that they can be used throughout the single- and two-phase regions.

Like in [9], we address here the problem of the phase appearance/disappearance through a single set of persistent variables, well adapted to heterogeneous porous media, which does not degenerate and hence could be used, without requiring switching the primary variables, as a unique formulation for both situations: liquid saturated and unsaturated. We will demonstrate, through four numerical tests, the ability of this new formulation to actually cope with the appearance or/and disappearance of one phase in simple but typical and challenging situations. Although these simulations are for demonstration purposes, they are however inspired from data given by some of the European Agencies looking at low permeability argillites as possible host rock for the geological underground storage of radioactive wastes, see [3, 18–20, 29–31, 36, 41]. Although the application we had in view for this model was the gas migration in geological radioactive waste repositories, we are aware that the very same problem of phase appearance and disappearance is also crucial in modeling the recently discussed technology of carbon capture and storage (see for instance [14, 15]).

2 Modeling physical assumptions

We consider herein a porous medium saturated with a fluid composed of two phases, *liquid* and *gas*, and according to the application we have in mind, we consider the fluid as a mixture of two components: water (only liquid) and hydrogen (H_2, mostly gas) or any gas with similar thermodynamical properties. In the following, for the sake of simplicity, we will call *hydrogen* the

nonwater component and use indices w and h for the *water* and the *hydrogen* components.

According to our goal, which was to focus on the phase appearance and disappearance phenomena, we have done several simplifying assumptions which are not essential for understanding our approach. Not doing these assumptions would have affected neither our choices of primary variables nor the conclusions, but they would have considerably complicated the present paper.

- The porous medium is assumed to be in thermal equilibrium. This hypothesis can be questionable in the case of application to nuclear waste repository where heat is generated by the nuclear waste, but, as argued in [8], the near-field thermal characteristic time is usually smaller than the corrosion time, so that most of the hydrogen production takes place when the system is close to thermal equilibrium. Hence, although thermal flux and energy conservation could be taken easily in account, for simplicity, they will not be discussed herein and we will consider only isothermal flows.
- After restoring thermal equilibrium in the repository and resaturation of the clay engineered barriers (in several hundred years, [8]), the water pressure far from the waste will be sufficiently high to prevent vapor formation. Near the waste, the gas phase will form, composed of the hydrogen and the water vapor. Since we are concerned with migration of the gas phase, which can happen only in the presence of higher pressure gradients, we assume that the presence of the vapor will not influence significantly the gas migration and therefore we neglect it in the modelization.
- Although at the depth of some storages, the water density could be affected by the pressure, we suppose for simplicity in our presentation that the water component is incompressible. For the very same reasons, the porous medium is supposed rigid, meaning that the porosity Φ is only a function of the space variable, $\Phi = \Phi(\mathbf{x})$.
- We are assuming that the gas flow can be described by the generalized two-phase Darcy's law, and we are not taking into account the possibility, in clayey rocks, of having the gas transported by other mechanism, see [33].

The two phases are denoted by indices, l for liquid and g for gas. Associated to each phase $\alpha \in \{\mathrm{l}, \mathrm{g}\}$, we have in the porous medium the phase pressures p_α, the phase saturations S_α, the phase mass densities ρ_α, and the phase volumetric fluxes $\mathbf{q}_\alpha$. The phase volumetric fluxes are given by the *Darcy–Muskat law* (see [5, 39]):

$$\begin{aligned} \mathbf{q}_\mathrm{l} &= -\mathbb{K}(\mathbf{x})\lambda_\mathrm{l}(S_\mathrm{l})\left(\nabla p_\mathrm{l} - \rho_\mathrm{l}\mathbf{g}\right), \\ \mathbf{q}_\mathrm{g} &= -\mathbb{K}(\mathbf{x})\lambda_\mathrm{g}(S_\mathrm{g})\left(\nabla p_\mathrm{g} - \rho_\mathrm{g}\mathbf{g}\right), \end{aligned} \tag{1}$$

where $\mathbb{K}(\mathbf{x})$ is the absolute permeability tensor, $\lambda_\alpha(S_\alpha)$ is the α-phase relative mobility function, and $\mathbf{g}$ is the gravitational acceleration; S_α is the effective α-phase saturation and then satisfies

$$S_\mathrm{l} + S_\mathrm{g} = 1. \tag{2}$$

Pressures are connected through a given *capillary pressure law* (see [6, 27]):

$$p_\mathrm{c}(S_\mathrm{g}) = p_\mathrm{g} - p_\mathrm{l}. \tag{3}$$

From definition (3), we notice that p_c is a strictly increasing function of gas saturation, $p_\mathrm{c}'(S_\mathrm{g}) > 0$, leading to a *capillary constraint*:

$$p_\mathrm{g} > p_\mathrm{l} + p_\mathrm{c}(0), \tag{4}$$

where $p_\mathrm{c}(0) \geq 0$ is the capillary curve entry pressure (see Fig. 2).

The water component and the gas component which are naturally in liquid state and in gas state at standard conditions are also denoted, respectively, as *solvent* and *solute*. We will assume herein, for simplicity, that the mixture contains only one solvent, the water, and one gas component, the hydrogen.

Writing all the quantities relative to one component with the superscript $i \in \{\mathrm{w}, \mathrm{h}\}$, we define then M^i as the molar mass of the i component and ρ_α^i, c_α^i, and X_α^i as, respectively, the dissolved mass, the dissolved molar densities, and the molar fraction of the i component in the α phase, $\alpha \in \{\mathrm{l}, \mathrm{g}\}$. All these quantities satisfy

$$\begin{aligned} &\rho_\alpha^i = M^i c_\alpha^i, \quad X_\alpha^i = \frac{c_\alpha^i}{c_\alpha}, \\ &\rho_\alpha = \sum_{k\in\{\mathrm{w},\mathrm{h}\}} \rho_\alpha^k, \quad c_\alpha = \sum_{k\in\{\mathrm{w},\mathrm{h}\}} c_\alpha^k. \end{aligned} \tag{5}$$

As said before, in the gas phase, we neglect the water vaporization and we use the ideal gas law (see [17]):

$$\rho_\mathrm{g} = C_\mathrm{v} p_\mathrm{g}, \tag{6}$$

with $C_\mathrm{v} = M^\mathrm{h}/(RT)$, where T is the temperature and R is the universal gas constant.

Mass conservation for each component leads to the following differential equations [2, 12]:

$$\Phi \frac{\partial}{\partial t}\left(S_\mathrm{l}\rho_\mathrm{l}^\mathrm{w}\right) + \mathrm{div}\left(\rho_\mathrm{l}^\mathrm{w}\mathbf{q}_\mathrm{l} + \mathbf{j}_\mathrm{l}^\mathrm{w}\right) = \mathscr{F}^\mathrm{w}, \tag{7}$$

$$\Phi \frac{\partial}{\partial t}\left(S_\mathrm{l}\rho_\mathrm{l}^\mathrm{h} + S_\mathrm{g}\rho_\mathrm{g}\right) + \mathrm{div}\left(\rho_\mathrm{l}^\mathrm{h}\mathbf{q}_\mathrm{l} + \rho_\mathrm{g}\mathbf{q}_\mathrm{g} + \mathbf{j}_\mathrm{l}^\mathrm{h}\right) = \mathscr{F}^\mathrm{h}, \tag{8}$$

where the phase flow velocities, $\mathbf{q}_l$ and $\mathbf{q}_g$, are given by the Darcy–Muskat law (1), $\mathscr{F}^k$ and $\mathbf{j}_l^k$, $k \in \{w, h\}$, are respectively the k-component source terms and the diffusive flux in the liquid phase (see (13)).

Assuming water incompressibility and independence of the liquid volume from the dissolved hydrogen concentration, we may assume the water component concentration in the liquid phase to be constant, i.e.,

$$\rho_l^w = \rho_w^{std}, \tag{9}$$

where ρ_w^{std} is the standard water mass density. The assumption of hydrogen thermodynamical equilibrium in both phases leads to equal chemical potentials in each phase: $\mu_g^h(T, p_g, X_g^h) = \mu_l^h(T, p_l, X_l^h)$. Assuming that in the gas phase there is only the hydrogen component and no water leads to $X_g^h = 1$, and then, from the above chemical potentials equality, we have a relationship $p_g = F(T, p_l, X_l^h)$. Assuming that the liquid pressure influence could be neglected in the pressure range considered herein and using the hydrogen low solubility, $\rho_l^h \ll \rho_l^w = \rho_w^{std}$, we may then linearize the solubility relation between p_g and X_l^h and obtain the *Henry's law* $p_g = K^h X_l^h$, where K^h is a constant specific to the mixture water/hydrogen and depends on the temperature T (see [17]). Furthermore, using (9) and the hydrogen low solubility, the molar fraction, X_l^h, reduces to $\frac{\rho_l^h M^w}{\rho_w^{std} M^h}$ (see (9)–(11) in [9]) and the Henry's law can be written as

$$\rho_l^h = C_h p_g, \tag{10}$$

where $C_h = HM^h = \rho_w^{std} M^h/(M^w K^h)$, where H is the Henry's law constant.

Remark 1 On the one hand, the gas pressure obeys the capillary pressure law (3) with the constraint (4), but on the other hand, it should also satisfy the local thermodynamical equilibrium and obey a solubility equation like the Henry's law (10). More precisely, if there are two phases, i.e., if the dissolved hydrogen mass density, ρ_l^h, is sufficiently high to lead to the appearance of a gas phase ($S_g > 0$), we have from (10) and (3)

$$\rho_l^h = C_h(p_l + p_c(S_g)). \tag{11}$$

Moreover, $S_g > 0$ with the capillary constraint (4) and the Henry's law (10) gives the solubility constraint:

$$\rho_l^h > C_h(p_l + p_c(0)). \tag{12}$$

But if the dissolved hydrogen mass density, ρ_l^h, is smaller than the concentration threshold (see Fig. 1), then there is only a liquid phase ($S_g = 0$) and none of all the relationships (3) or (12), connected to capillary equilibrium, apply anymore; we have only $S_g = 0$, with $\rho_l^h \le C_h p_g$.

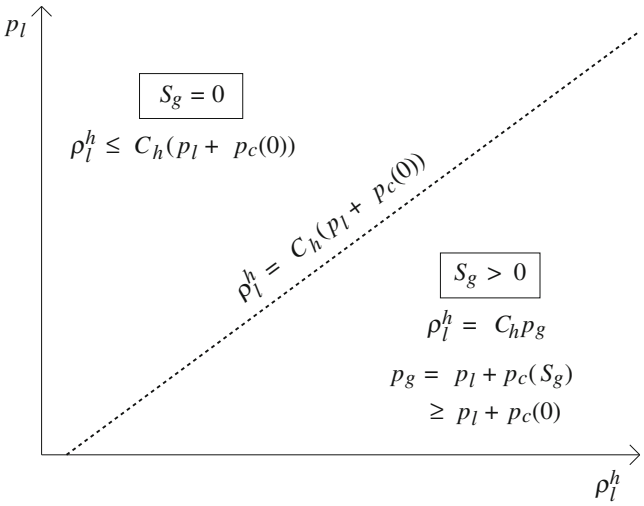

Fig. 1 Phase diagram: Henry's law. Localization of the liquid saturated $S_g = 0$ and unsaturated $S_g > 0$ states

The concentration threshold line, $\rho_l^h = C_h(p_l + p_c(0))$ in the phase diagram, is then separating the one-phase (liquid saturated) region from the two-phase (unsaturated) region.

The existence of a concentration threshold line can also be written as unilateral conditions:

$$0 \le S_g \le 1, \quad 0 \le \rho_l^h \le C_h p_g, \quad S_g(C_h p_g - \rho_l^h) = 0,$$

which could be added to the conservation laws (7) and (8) and solved conjointly at each time step by means of a semismooth Newton's method, as explained in Section 1 and in [22] or [26].

Since hydrogen is highly diffusive, we include the dissolved hydrogen diffusion in the liquid phase. The diffusive fluxes in the liquid phase are given by the Fick's law applied to X_l^w and to X_l^h, the water component and the hydrogen component molar fractions (see (12) and (13) in [9]). Using the same kind of approximation as in the Henry's law, based on the hydrogen low solubility,

we obtain, for the diffusive fluxes in this binary mixture (see Remarks 2 and 3 in [9] and see [7]),

$$\mathbf{j}_l^h = -\Phi S_l D \nabla \rho_l^h, \quad \mathbf{j}_l^w = -\mathbf{j}_l^h, \tag{13}$$

where D is the hydrogen molecular diffusion coefficient in the liquid phase, possibly corrected by the tortuosity factor of the porous medium (see [23, 40]).

If both liquid and gas phases exist ($S_g \neq 0$), the porous medium is said to be *unsaturated*, then the transport model for the liquid–gas system can be obtained from (1), (7), and (8), using (5), (6), (9), and (13),

$$\Phi\rho_w^{std}\frac{\partial S_l}{\partial t} + \mathrm{div}\left(\rho_w^{std}\mathbf{q}_l - \mathbf{j}_l^h\right) = \mathscr{F}^w, \tag{14}$$

$$\Phi\frac{\partial}{\partial t}(S_l\rho_l^h + C_v p_g S_g) + \mathrm{div}\left(\rho_l^h\mathbf{q}_l + C_v p_g\mathbf{q}_g + \mathbf{j}_l^h\right) = \mathscr{F}^h, \tag{15}$$

$$\mathbf{q}_l = -\mathbb{K}\lambda_l(S_l)\left(\nabla p_l - (\rho_w^{std} + \rho_l^h)\mathbf{g}\right), \tag{16}$$

$$\mathbf{q}_g = -\mathbb{K}\lambda_g(S_g)\left(\nabla p_g - C_v p_g\mathbf{g}\right), \tag{17}$$

$$\mathbf{j}_l^h = -\Phi S_l D\nabla\rho_l^h. \tag{18}$$

But in the *liquid saturated* regions, where the gas phase does not appear, $S_l = 1$, the system (14)–(18) degenerates to

$$\mathrm{div}\left(\rho_w^{std}\mathbf{q}_l - \mathbf{j}_l^h\right) = \mathscr{F}^w, \tag{19}$$

$$\Phi\frac{\partial\rho_l^h}{\partial t} + \mathrm{div}\left(\rho_l^h\mathbf{q}_l + \mathbf{j}_l^h\right) = \mathscr{F}^h, \tag{20}$$

$$\mathbf{q}_l = -\mathbb{K}\lambda_l(1)\left(\nabla p_l - (\rho_w^{std} + \rho_l^h)\mathbf{g}\right), \tag{21}$$

$$\mathbf{j}_l^h = -\Phi D\nabla\rho_l^h. \tag{22}$$

3 Liquid saturated/unsaturated state: a general formulation

As recalled in Section 1, a traditional choice for the primary unknowns, in modeling two-phase flow and transport process, is the saturation and one of the phases' pressure, for example, S_g and p_l. But as seen above, in (19)–(22), saturation is no longer a consistent variable in saturated regions and this set of unknowns cannot describe the flow in a region where there is only one phase (see [43]). In this section, we present and compare two possible choices of primary variables to circumvent this difficult problem, namely:

- One already presented in [9], using liquid pressure and total hydrogen mass density, well adapted when the capillary forces are negligible, which is the case in most enhanced oil recovery simulations;
- A new variant of primary variable, suitable only if capillary forces are important, compatible at the same time with phase transitions and computations in heterogeneous media.

In the following sections, we consider only this new variant of primary variable (the first one was already considered in [9]) for numerical applications and discussion of examples.

3.1 Modeling based on the total hydrogen mass density, ρ_{tot}^h

To solve this problem, instead of using the gas saturation S_g we have proposed, in [9], to use ρ_{tot}^h, the total hydrogen mass density, defined as

$$\rho_{tot}^h = S_l\rho_l^h + S_g\rho_g^h. \tag{23}$$

Then, defining

$$a(S_g) = C_h(1 - S_g) + C_v S_g \in [C_h, C_v], \tag{24}$$

with

$$a'(S_g) = C_v - C_h = C_\Delta > 0, \tag{25}$$

since $C_v > C_h$, from the assumption of weak solubility, we may rewrite the total hydrogen mass density, ρ_{tot}^h, defined in (23), as

$$\rho_{tot}^h = \begin{cases} a(S_g)(p_l + p_c(S_g)) & \text{if } S_g > 0 \\ \rho_l^h & \text{if } S_g = 0. \end{cases} \tag{26}$$

As noticed in the previous section in Remark 1, using the monotonicity of functions $p_c(S_g)$ and $a(S_g)$, we see a concentration threshold corresponding to $C_h(p_l + p_c(0))$ separating the liquid saturated zone, $\rho_{tot}^h \leq C_h(p_l + p_c(0))$, from the unsaturated zone, $\rho_{tot}^h > C_h(p_l + p_c(0))$.

With this choice of primary variables, ρ_{tot}^h and p_l, the two systems of (14)–(18) and (19)–(22) reduce to a single system of equations:

$$\Phi\rho_w^{std}\frac{\partial S_l}{\partial t} - \mathrm{div}\left(\rho_w^{std}\mathbb{K}\lambda_l(S_l)\left(\nabla p_l - (\rho_w^{std} + \rho_l^h)\mathbf{g}\right)\right) + \mathrm{div}\left(\Phi S_l D\nabla\rho_l^h\right) = \mathscr{F}^w, \tag{27}$$

$$\Phi\frac{\partial\rho_{tot}^h}{\partial t} - \mathrm{div}\left(\rho_l^h\mathbb{K}\lambda_l(S_l)\left(\nabla p_l - (\rho_w^{std} + \rho_l^h)\mathbf{g}\right)\right) - \mathrm{div}\left(C_v p_g\mathbb{K}\lambda_g(S_g)\left(\nabla p_l + \nabla p_c(S_g) - C_v p_g\mathbf{g}\right)\right) - \mathrm{div}\left(\Phi S_l D\nabla\rho_l^h\right) = \mathscr{F}^h. \tag{28}$$

If we want to study the mathematical properties of the operators in this system of equations, we should develop the above system of equations using first the dependency of the secondary variables $S_g = S_g(p_l, \rho^h_{tot})$, $S_l = 1 - S_g = S_l(p_l,\ \rho^h_{tot})$, and $\rho^h_l = \rho^h_l(p_l, \rho^h_{tot})$ and secondly computing the derivatives of the saturations, from (26),

$$\frac{\partial S_g}{\partial p_l} = -\frac{a(S_g)^2 \mathbb{1}_{\{\rho^h_{tot} > C_h(p_l + p_c(0))\}}}{C_\Delta \rho^h_{tot} + a(S_g)^2 p'_c(S_g)}, \tag{29}$$

$$\frac{\partial S_g}{\partial \rho^h_{tot}} = \frac{a(S_g) \mathbb{1}_{\{\rho^h_{tot} > C_h(p_l + p_c(0))\}}}{C_\Delta \rho^h_{tot} + a(S_g)^2 p'_c(S_g)}, \tag{30}$$

where $\mathbb{1}_{\{\rho^h_{tot} > C_h(p_l + p_c(0))\}}$ is the characteristic function of the set $\{\rho^h_{tot} > C_h(p_l + p_c(0))\}$.

As noted in Section 2.5 in [9], we have $\partial S_g/\partial p_l \leq 0$ and $\partial S_g/\partial \rho^h_{tot} > 0$, when the gas phase is present. Then, the system (14) and (15) can be written as

$$-\Phi \rho^{std}_w \frac{\partial S_g}{\partial p_l}\frac{\partial p_l}{\partial t} - \mathrm{div}\left(\mathbb{A}^{1,1}\nabla p_l + \mathbb{A}^{1,2}\nabla \rho^h_{tot} + B_1 \mathbb{K}\mathbf{g}\right) - \Phi \rho^{std}_w \frac{\partial S_g}{\partial \rho^h_{tot}}\frac{\partial \rho^h_{tot}}{\partial t} = \mathscr{F}^w \tag{31}$$

$$\Phi \frac{\partial \rho^h_{tot}}{\partial t} - \mathrm{div}\left(\mathbb{A}^{2,1}\nabla p_l + \mathbb{A}^{2,2}\nabla \rho^h_{tot} + B_2 \mathbb{K}\mathbf{g}\right) = \mathscr{F}^h, \tag{32}$$

where the coefficients are defined by

$$\mathbb{A}^{1,1}(p_l, \rho^h_{tot}) = \lambda_l(S_l)\rho^{std}_w \mathbb{K} - \Phi S_l D C_h N \mathbb{I}, \tag{33}$$

$$\mathbb{A}^{1,2}(p_l, \rho^h_{tot}) = -\Phi S_l \frac{1-N}{a(S_g)} D C_h \mathbb{I}, \tag{34}$$

$$\mathbb{A}^{2,1}(p_l, \rho^h_{tot}) = (\lambda_l(S_l)\rho^h_l + \lambda_g(S_g) C_v p_g N)\mathbb{K} + \Phi S_l D C_h N \mathbb{I}, \tag{35}$$

$$\mathbb{A}^{2,2}(p_l, \rho^h_{tot}) = \frac{1-N}{a(S_g)}\left\{\lambda_g(S_g) C_v p_g \mathbb{K} + \Phi S_l D C_h \mathbb{I}\right\} \tag{36}$$

$$B_1(p_l, \rho^h_{tot}) = -\lambda_l(S_l)\rho^{std}_w[\rho^{std}_w + \rho^h_l], \tag{37}$$

$$B_2(p_l, \rho^h_{tot}) = -(\lambda_l(S_l)\rho^h_l[\rho^{std}_w + \rho^h_l] + \lambda_g(S_g) C_v^2 p_g^2), \tag{38}$$

with $\mathbb{I}$ denoting the identity matrix and with the auxiliary functions

$$N(p_l, \rho^h_{tot}) = \frac{C_\Delta \rho^h_{tot}}{C_\Delta \rho^h_{tot} + a(S_g)^2 p'_c(S_g)} \tilde{\mathbb{1}} \in [0, 1),$$
$$\tilde{\mathbb{1}} = \mathbb{1}_{\{\rho^h_{tot} > C_h(p_l + p_c(0))\}} \tag{39}$$

$$\rho^h_l(p_l, \rho^h_{tot}) = \min(C_h p_g(p_l, \rho^h_{tot}), \rho^h_{tot}), \tag{40}$$

$$p_g(p_l, \rho^h_{tot}) = p_l + p_c(S_g(p_l, \rho^h_{tot})). \tag{41}$$

We should notice first that (32) is uniformly parabolic in the presence of capillarity and diffusion, but if capillarity and diffusion are neglected, this same equation becomes a pure hyperbolic transport equation (see Section 2.6 in [9]). Then, if we sum (31) and (32), we obtain a uniformly parabolic/elliptic equation, which is parabolic in the unsaturated (two-phase) region and elliptic in the liquid saturated (one-phase) region.

Remark 2 Simulations presented in Section 3.2 in [9] show that this last choice of primary variables, ρ^h_{tot} and p_l, could easily handle phase transitions (appearance/disappearance of the gas phase, saturated zones, etc.) in two-phase partially miscible flows. However, the discontinuity of the characteristic function with respect to the main variable ρ^h_{tot}, on the concentration threshold line, $\mathbb{1}_{\{\rho^h_{tot} > C_h(p_l + p_c(0))\}}$, in (29), (30), and (39), has some effect on the conditioning of the Jacobian matrix and hence on the number of Newton iterations and the number of iterations required to solve the Jacobian system, except if the fraction in front of the characteristic function in (39) tends to zero as $S_g \to 0$, which is the case when the van Genuchten's capillary curves are used.

Another variant is presented in [1], where using the total hydrogen concentration,

$$C^h_{tot} = \frac{(1-S_g)\rho^h_l + S_g \rho_g}{(1-S_g)\rho_l + S_g \rho_g}; \tag{42}$$

an extended saturation can be defined from the inverse of (42):

$$S_g = \frac{C^h_{tot}\rho_l - \rho^h_l}{C^h_{tot}\rho_l - \rho^h_l + (1-C)\rho_g}. \tag{43}$$

This saturation which was initially defined in the two-phase region is then extended outside this region by doing $\rho_g = \rho_l$ in (42), since, no matter in what region we are, there exists always an "extended" saturation

($S_g \leq 0$, outside the two-phase region), which can be chosen as primary variable. It is then possible to model both the one-phase flow and the two-phase flow with the same system of equations written with this extended saturation as the main unknown, and the gas appearance and disappearance is actually treated through the total hydrogen concentration C^h_{tot} expression (see [32]).

3.2 Modeling based on the dissolved hydrogen mass density in the liquid phase, ρ_l^h

We have seen that the variables p_l and ρ^h_{tot}, introduced in the last section, describe the flow system, both in the one-phase and in the two-phase regions, independently of the presence of diffusion or capillary forces. But if we assume moreover that the effects of the capillary forces are not negligible, we can choose an other set of primary variables.

Namely, using the retention curve (inverse of the capillary pressure curve), we may define the phase saturation as function of the dissolved hydrogen mass density in the liquid, ρ_l^h, and of the liquid pressure, p_l, and hence use them as main unknowns. With these two variables, ρ_l^h and p_l, the two systems (14)–(18) and (19)–(22) are transformed in a single system of equations able to describe both liquid saturated and unsaturated flows.

Since the capillary pressure curve $S_g \mapsto p_c(S_g)$ is a strictly increasing function, we can define an inverse function (retention curve) $f : \mathbb{R} \to [0, 1]$ (see Fig. 2), by

$$f(\pi) = \begin{cases} p_c^{-1}(\pi) & \text{if } \pi \geq p_c(0) \\ 0 & \text{otherwise.} \end{cases} \tag{44}$$

By definition of the retention curve f, using (10) and (12), we have

$$f\left(\frac{\rho_l^h}{C_h} - p_l\right) = S_g, \tag{45}$$

and it is then possible to compute the gas saturations, S_g, from p_l and ρ_l^h. With these two variables being well defined in both the one- and two-phase regimes, we will now use them as principal unknowns.

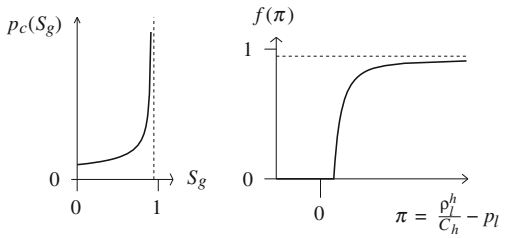

Fig. 2 Capillary pressure curve, $p_c = p_g - p_l$, and inverse function

Equations (14)–(18) with unknowns p_l and ρ_l^h can be written as

$$-\Phi\rho_w^{std}\frac{\partial}{\partial t}\left(f\left(\frac{\rho_l^h}{C_h} - p_l\right)\right) - \operatorname{div}\left(\tilde{\mathbb{A}}^{1,1}\nabla p_l + \tilde{\mathbb{A}}^{1,2}\nabla\rho_l^h + B_1\mathbb{K}\mathbf{g}\right) = \mathscr{F}^w, \tag{46}$$

$$\Phi\frac{\partial}{\partial t}\left(a^* \circ f\left(\frac{\rho_l^h}{C_h} - p_l\right)\rho_l^h\right) - \operatorname{div}\left(\tilde{\mathbb{A}}^{2,1}\nabla p_l + \tilde{\mathbb{A}}^{2,2}\nabla\rho_l^h + B_2\mathbb{K}\mathbf{g}\right) = \mathscr{F}^h, \tag{47}$$

where the coefficients are given by the following formulas:

$$\tilde{\mathbb{A}}^{1,1} = \lambda_l(S_l)\rho_w^{std}\mathbb{K}, \quad \tilde{\mathbb{A}}^{1,2} = -\Phi S_l D\mathbb{I}, \tag{48}$$

$$\tilde{\mathbb{A}}^{2,1} = \lambda_l(S_l)\rho_l^h\mathbb{K}, \quad \tilde{\mathbb{A}}^{2,2} = \lambda_g(S_g)\frac{C_v}{C_h^2}\rho_l^h\mathbb{K} + \Phi S_l D\mathbb{I}, \tag{49}$$

with B_1 and B_2 defined as in (37), (38), and

$$a^*(S_g) = \frac{a(S_g)}{C_h} = 1 + \left(\frac{C_v}{C_h} - 1\right)S_g. \tag{50}$$

If we consider first (47), we may write it as

$$\Phi\left(a^*(S_g) + \rho_l^h\frac{\partial a^*(S_g)}{\partial\rho_l^h}\right)\frac{\partial\rho_l^h}{\partial t} - \operatorname{div}\left(\tilde{\mathbb{A}}^{2,1}\nabla p_l + \tilde{\mathbb{A}}^{2,2}\nabla\rho_l^h + B_2\mathbb{K}\mathbf{g}\right) + \Phi\rho_l^h\frac{\partial a^*(S_g)}{\partial p_l}\frac{\partial p_l}{\partial t} = \mathscr{F}^h.$$

Moreover, from (50) and because f and f' are positive, we have

$$a^*(S_g) + \rho_l^h\frac{\partial a^*(S_g)}{\partial\rho_l^h} = 1 + \left(\frac{C_v}{C_h} - 1\right)\left(f\left(\frac{\rho_l^h}{C_h} - p_l\right) + \frac{\rho_l^h}{C_h}f'\left(\frac{\rho_l^h}{C_h} - p_l\right)\right) \geq 1,$$

and if the diffusion is not neglected, we have definite positiveness of the quadratic form $\tilde{\mathbb{A}}^{2,2}$, in (47), i.e., for any $\boldsymbol{\xi} \neq 0$,

$$(\tilde{\mathbb{A}}^{2,2}\boldsymbol{\xi}\cdot\boldsymbol{\xi}) = \lambda_g(S_g)\frac{C_v}{C_h^2}\rho_l^h\mathbb{K}\boldsymbol{\xi}\cdot\boldsymbol{\xi} + \Phi(1 - S_g)D|\boldsymbol{\xi}|^2 > 0,$$

and therefore (47) is strictly parabolic in ρ_l^h.

If we develop (46) as follows

$$\Phi\rho_{\mathrm{w}}^{\mathrm{std}} f'\left(\frac{\rho_{\mathrm{l}}^{\mathrm{h}}}{C_{\mathrm{h}}} - p_{\mathrm{l}}\right)\frac{\partial p_{\mathrm{l}}}{\partial t} - \mathrm{div}\big(\tilde{\mathbb{A}}^{1,1}\nabla p_{\mathrm{l}} + \tilde{\mathbb{A}}^{1,2}\nabla\rho_{\mathrm{l}}^{\mathrm{h}} + B_{\mathrm{l}}\mathbb{K}\mathbf{g}\big) - \frac{\rho_{\mathrm{w}}^{\mathrm{std}}}{C_{\mathrm{h}}}\Phi f'\left(\frac{\rho_{\mathrm{l}}^{\mathrm{h}}}{C_{\mathrm{h}}} - p_{\mathrm{l}}\right)\frac{\partial\rho_{\mathrm{l}}^{\mathrm{h}}}{\partial t} = \mathscr{F}^{\mathrm{w}},$$

we have, for any $\boldsymbol{\xi}$,

$$\lambda_{\mathrm{l}}(S_{\mathrm{l}})\rho_{\mathrm{w}}^{\mathrm{std}}\mathbb{K}\boldsymbol{\xi}\cdot\boldsymbol{\xi} \geq 0,$$

and then positiveness of $(\tilde{\mathbb{A}}^{1,1}\boldsymbol{\xi}\cdot\boldsymbol{\xi})$ and of $(\tilde{\mathbb{A}}^{2,1}\boldsymbol{\xi}\cdot\boldsymbol{\xi})$.

Moreover,

$$\Phi\rho_{\mathrm{w}}^{\mathrm{std}} f'\left(\frac{\rho_{\mathrm{l}}^{\mathrm{h}}}{C_{\mathrm{h}}} - p_{\mathrm{l}}\right) \geq 0.$$

However, equations in system (46) and (47) are not uniformly parabolic/elliptic for the pressure p_{l}, because the coefficients, $\tilde{\mathbb{A}}^{1,1}$, $\tilde{\mathbb{A}}^{2,1}$, in front of ∇p_{l} in (46) and (47) tend to zero as $S_{\mathrm{g}} \to 1$.

Remark 3 It is worth noticing that this system (46) and (47), with variables p_{l} and $\rho_{\mathrm{l}}^{\mathrm{h}}$, has interesting properties for numerical simulations in strongly heterogeneous porous media. These two variables are continuous through interfaces separating different porous media with different rock types (different absolute permeability, different capillary and permeability curves), as we will see in Section 4.3, which is not the case for the total hydrogen density $\rho_{\mathrm{tot}}^{\mathrm{h}}$. Another advantage is the continuity, in the neighborhood of the concentration threshold line, of all the coefficients $\tilde{\mathbb{A}}^{i,j}$, in (46) and (47) and of f in (47). However, the choice of total hydrogen mass density, $\rho_{\mathrm{tot}}^{\mathrm{h}}$, for the primary variable does not require capillary effects, making it useful when the capillary effects are negligible, which is not the case with the choice of the dissolved hydrogen density, $\rho_{\mathrm{l}}^{\mathrm{h}}$, as the primary variable, which is relying on an invertible capillary pressure curve (see (45)). Moreover, with this choice of $\rho_{\mathrm{l}}^{\mathrm{h}}$, as the primary variable, steepest or infinite slope in the capillary curve or in the retention curve has an effect on the conditioning of the Jacobian and makes a problem for computing back the secondary variables.

Remark 4 From the solubility equation given by the Henry's law (10), it is possible to define an "extended" gas pressure by $\tilde{p}_{\mathrm{g}} = \rho_{\mathrm{l}}^{\mathrm{h}}/C_{\mathrm{h}}$ even inside the liquid saturated region. Obviously, this extended gas pressure coincides with the true gas pressure p_{g} in the two-phase region. In [4] and [35], this extended gas pressure and the liquid pressure are chosen for primary variables and the gas appearance and disappearance is treated through the retention curve.

4 Numerical experiments

In this last section, we present four numerical tests specially designed for illustrating the ability of the model described by (46) and (47) to deal with gas phase appearance and disappearance. All the computations were done using the variables p_{l} and $\rho_{\mathrm{l}}^{\mathrm{h}}$; we are also displaying, for each test, the saturation and pressure level curves. These two last quantities are obtained after a post-processing step using the capillary pressure law (3), (45), Henry's law (10), and the constraints (4) and (12) (see Fig. 1).

The first test focuses on the gas phase appearance produced by injecting pure hydrogen in a 2-D homogeneous porous domain Ω (see Fig. 3), which is initially liquid-saturated by pure water.

Because the main goal of all these numerical experiments is to test the model efficiency, for describing the phase appearance or disappearance, the porous domain geometry does not really matter and we will use a porous domain with a simple geometry. Consequently, we choose a simple, quasi-1-D, porous domain (see Fig. 4) for the following three tests.

The test case number 2 is more complex; it shows local disappearance of the gas phase created by injecting pure hydrogen in a homogeneous unsaturated porous medium (initially both phases, liquid and gas, are present everywhere).

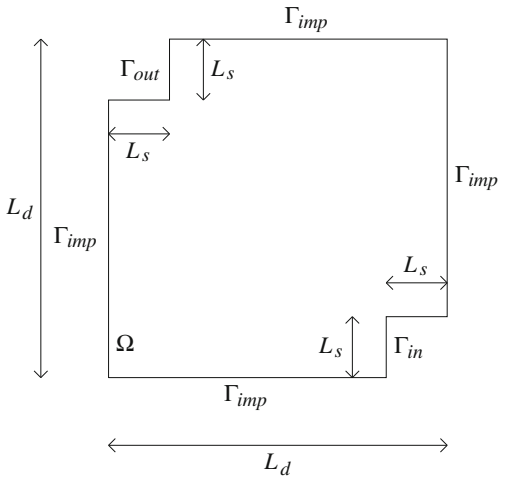

Fig. 3 Test case number 1: Geometry a the 2-D porous domain, Ω

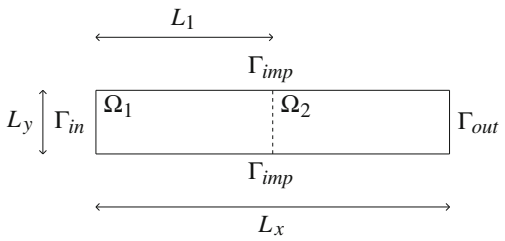

Fig. 4 Test cases number 2, 3, and 4: Geometry of the quasi-1-D porous domain, $\overline{\Omega} = \overline{\Omega_1} \cup \overline{\Omega_2}$

The two last tests' aim is to focus on the main challenges in simulating the flow crossing the engineered barriers, located around the waste packages. In test case number 3, the porous medium domain is split in two parts with different and highly contrasted rock types, and like in the first one, the gas phase appearance is produced by injecting pure hydrogen in an initially water-saturated porous domain. Test case number 4 addresses the evolution of the phases, from an initial phase disequilibrium to a stabilized stationary state, in a closed porous domain (no-flux boundary conditions).

In all these four test cases, for simplicity, the porous medium is assumed to be isotropic, such that $\mathbb{K} = k\mathbb{I}$ with k as a positive scalar, and the source terms are assumed to be null: $\mathscr{F}_{\mathrm{w}} = 0$ and $\mathscr{F}_{\mathrm{h}} = 0$. As usual, in hydrogeology, the van Genuchten–Mualem model for the capillary pressure law and the relative permeability functions (see [28, 42]) are used for underground nuclear waste modeling, i.e.,

$$\begin{cases} p_{\mathrm{c}} = P_{\mathrm{r}} \left(S_{\mathrm{le}}^{-1/m} - 1 \right)^{1/n}, \\ \lambda_{\mathrm{l}} = \dfrac{1}{\mu_{\mathrm{l}}} \sqrt{S_{\mathrm{le}}} \left(1 - (1 - S_{\mathrm{le}}^{1/m})^m \right)^2 \\ \text{and} \quad \lambda_{\mathrm{g}} = \dfrac{1}{\mu_{\mathrm{g}}} \sqrt{1 - S_{\mathrm{le}}} \left(1 - S_{\mathrm{le}}^{1/m} \right)^{2m} \\ \text{with} \quad S_{\mathrm{le}} = \dfrac{S_{\mathrm{l}} - S_{\mathrm{l,res}}}{1 - S_{\mathrm{l,res}} - S_{\mathrm{g,res}}} \quad \text{and} \quad m = 1 - \dfrac{1}{n}. \end{cases} \tag{51}$$

Table 1 Fluid parameters: phase and component characteristics

Parameter	Value
θ	303 K
$D_{\mathrm{l}}^{\mathrm{h}}$	$3 \cdot 10^{-9}$ m^2/s
μ_{l}	$1 \cdot 10^{-3}$ Pa s
μ_{g}	$9 \cdot 10^{-6}$ Pa s
$H(\theta = 303\ \mathrm{K})$	$7.65 \cdot 10^{-6}$ mol/Pa/m^3
M^{w}	18 g/mol
M^{h}	$2 \cdot 10^{-3}$ kg/mol
$\rho_{\mathrm{w}}^{\mathrm{std}}$	10^3 kg/m^3

Table 2 Mesh sizes and time steps used in the different numerical tests

	Mesh size range	Time step range
Test number 1	2–6 m[a]	10^2–$5 \cdot 10^4$ years
Test number 2	1 m[b]	10^2–$5 \cdot 10^3$ years
Test number 3	1 m[b]	10^2–$2 \cdot 10^4$ years
Test number	$2 \cdot 10^{-3}$ m[b]	0.33–$16.7 \cdot 10^3$ s

[a]Unstructured triangular mesh
[b]Regular quadrangular mesh

Note that in the van Genuchten–Mualem model, there is no capillary pressure jump at 0, $p_{\mathrm{c}}(0) = 0$, but the presence of a jump, like in the Brooks–Corey model (see [10]), would not lead to any difficulty, neither from the mathematical point of view nor for the numerical simulations. Concerning the other fluid characteristics, the values of the physical parameters specific to the phases (liquid and gas) and to the components (water and hydrogen) are given in Table 1. All the simulations, presented herein, were performed using the modular code *Cast3m* [11], with the nonlinear differential equation system discretized with a full implicit time scheme. The nonlinearities were treated by a Newton method with an incomplete Jacobian (some derivatives in $A_{i,j}$ and B_j were neglected), and the obtained sequences of linear differential equations were discretized by a finite-volume scheme. The discretization parameters (mesh size and time step) are given in Table 2.

4.1 Numerical test number 1

The geometry of this test case is given in Fig. 3, and the related data are given in Table 3. A constant flux of hydrogen is imposed on the input boundary, Γ_{in}, while Dirichlet conditions $p_{\mathrm{l}} = p_{\mathrm{l,out}}$, $\rho_{\mathrm{l}}^{\mathrm{h}} = 0$ are given on Γ_{out}

Table 3 Numerical test case number 1: boundary and initial conditions, porous medium characteristics, and domain geometry; ϕ^{w} and ϕ^{h} are denoting respectively the water and hydrogen flux

Boundary conditions	Porous medium	
Initial condition	Parameter	Value
$\phi^{\mathrm{w}} \cdot \nu = 0$ on Γ_{imp}	k	$5 \cdot 10^{-20}$ m^2
$\phi^{\mathrm{h}} \cdot \nu = 0$ on Γ_{imp}	Φ	0.15
$\phi^{\mathrm{w}} \cdot \nu = 0$ on Γ_{in}	P_{r}	$2 \cdot 10^6$ Pa
$\phi^{\mathrm{h}} \cdot \nu = \mathscr{Q}^{\mathrm{h}}$ on Γ_{in}	n	1.49
$p_{\mathrm{l}} = p_{\mathrm{l,out}}$ on Γ_{out}	$S_{\mathrm{l,res}}$	0.4
$\rho_{\mathrm{l}}^{\mathrm{h}} = 0$ on Γ_{out}	$S_{\mathrm{g,res}}$	0
$p_{\mathrm{l}}(t = 0) = p_{\mathrm{l,out}}$ in Ω	Others	
$\rho_{\mathrm{l}}^{\mathrm{h}}(t = 0) = 0$ in Ω	Parameter	Value
$p_{\mathrm{l,out}} = 10^6$ Pa	L_{d}	200 m
	L_{s}	20 m
	$\mathscr{Q}^{\mathrm{h}}$	9.28 mg/m^2/year

in order to have only the water component on this part of the boundary. The initial conditions, $p_\mathrm{l} = p_{\mathrm{l,out}}$ and $\rho_\mathrm{l}^\mathrm{h} = 0$, are uniform on all the domain and correspond to a porous domain initially saturated with pure water.

The main steps of the corresponding simulation are presented in Fig. 5.

We observe in the beginning (see time $t =$ 1,200 years in Fig. 5) that all the injected hydrogen through Γ_{in} is totally dissolved in the liquid phase; the gas saturation stays null on all the domain (there is no gas phase). During that same period of time, the increase in liquid pressure is relatively small, the liquid phase flux originates slowly (they are both hard to see on the figures), and the hydrogen is transported mainly by diffusion of the dissolved hydrogen in the liquid phase.

Later on, the dissolved hydrogen accumulates around Γ_{in} until the dissolved hydrogen mass density $\rho_\mathrm{l}^\mathrm{h}$ reaches the threshold $\rho_\mathrm{l}^\mathrm{h} = C_\mathrm{h} p_\mathrm{l}$ (according to Fig. 1 and $p_\mathrm{c}(0) = 0$ in Remark 1), at time $t = 1{,}600$ years, when the gas phase appears in the vicinity of Γ_{in}. Then, this unsaturated region progressively expands. The gas phase volume expansion creates a gradient of the liquid pressure in the porous domain, causing the liquid

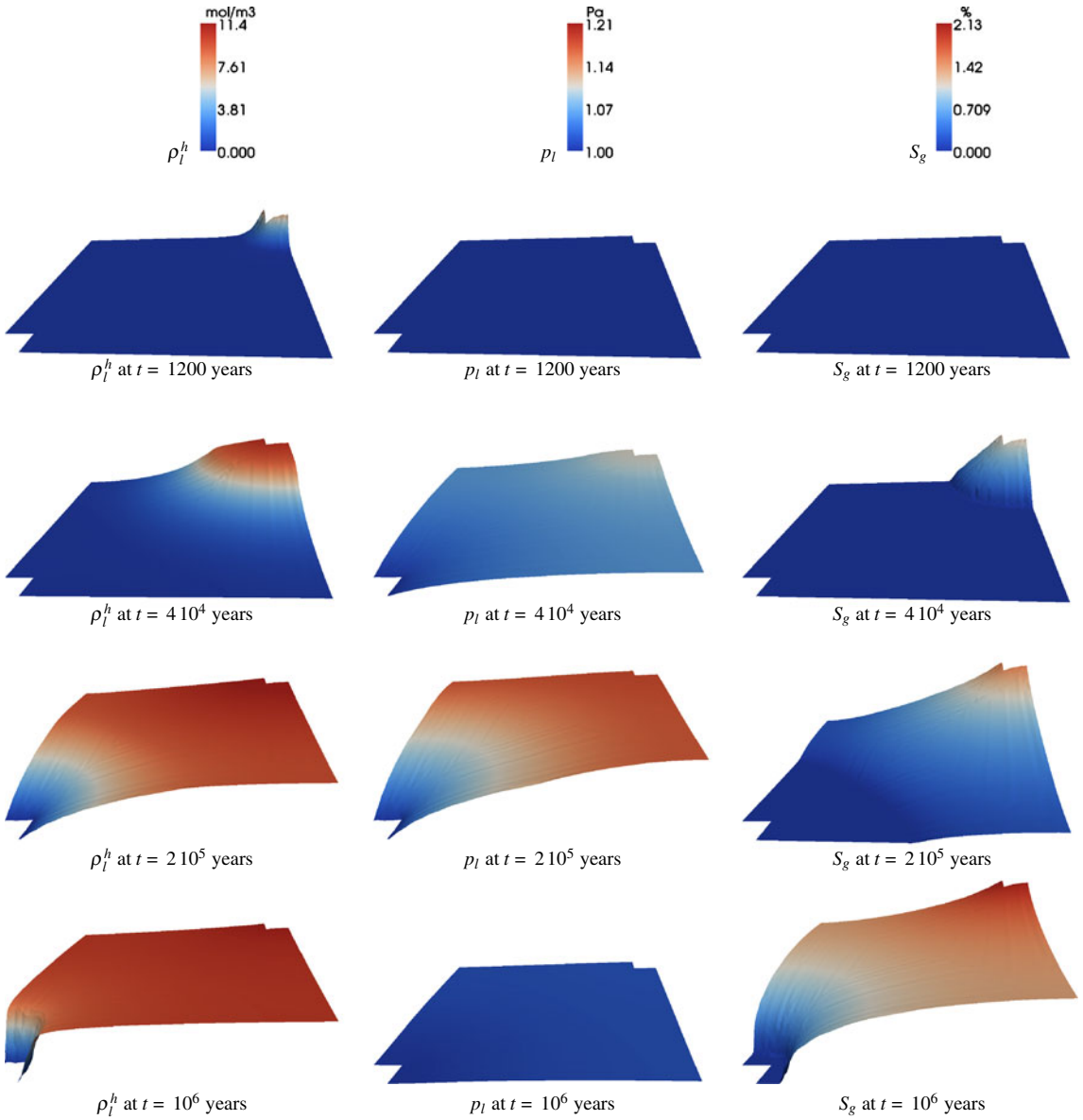

Fig. 5 Numerical test case number 1: Evolution of $\rho_\mathrm{l}^\mathrm{h}$, the hydrogen density in the liquid phase; p_l, the liquid phase pressure; and S_g, the gas saturation at times $t = 1{,}200, 4 \cdot 10^4, 2 \cdot 10^5$, and 10^6 years (from the *top* to *bottom*)

Table 4 Numerical test case number 2: boundary and initial conditions, porous medium characteristics, and domain geometry

Boundary conditions	Porous medium	
Initial condition	Parameter	Value
$\phi^{\mathrm{w}} \cdot \nu = 0$ on Γ_{imp}	k	$5 \cdot 10^{-20}$ m^2
$\phi^{\mathrm{h}} \cdot \nu = 0$ on Γ_{imp}	Φ	0.15
$\phi^{\mathrm{w}} \cdot \nu = 0$ on Γ_{in}	P_{r}	$2 \cdot 10^6$ Pa
$\phi^{\mathrm{h}} \cdot \nu = \mathscr{Q}^{\mathrm{h}}$ on Γ_{in}	n	1.49
$p_{\mathrm{l}} = p_{\mathrm{l,out}}$ on Γ_{out}	$S_{\mathrm{l,res}}$	0.4
$\rho_{\mathrm{l}}^{\mathrm{h}} = C_{\mathrm{h}} p_{\mathrm{g,out}}$ on Γ_{out}	$S_{\mathrm{g,res}}$	0
$p_{\mathrm{l}}(t=0) = p_{\mathrm{l,out}}$ in Ω	Others	
$\rho_{\mathrm{l}}^{\mathrm{h}}(t=0) = C_{\mathrm{h}} p_{\mathrm{g,out}}$ in Ω	Parameter	Value
$p_{\mathrm{l,out}} = 10^6$ Pa	L_x	200 m
$p_{\mathrm{g,out}} = 1.1 \cdot 10^6$ Pa	L_y	20 m
$\mathscr{Q}^{\mathrm{h}} = 55.7$ mg/m^2/year	L_1	0 m

ϕ^{w} and ϕ^{h} are denoting respectively the water and hydrogen flux

phase to flow from Γ_{in} to Γ_{out}. Consequently, after this time, $t = 1{,}600$ years, the hydrogen is transported by convection in the gas phase and the dissolved hydrogen is transported by both convection and diffusion in the liquid phase. The liquid phase pressure increases globally in the whole domain until time $t = 260{,}000$ years (see Fig. 5). Then, it starts to decrease in the whole domain until reaching a uniform and stationary state at $t = 10^6$ years, corresponding everywhere to a null water component flux. Note that in this stationary state, $\rho_{\mathrm{l}}^{\mathrm{h}}$ still slightly varies (not only around the outflow corner), and because of very small value of the Henry's constant C_{h} in (10), this variation produces by (45) noticeable gas saturation variation, which can be observed in Fig. 5.

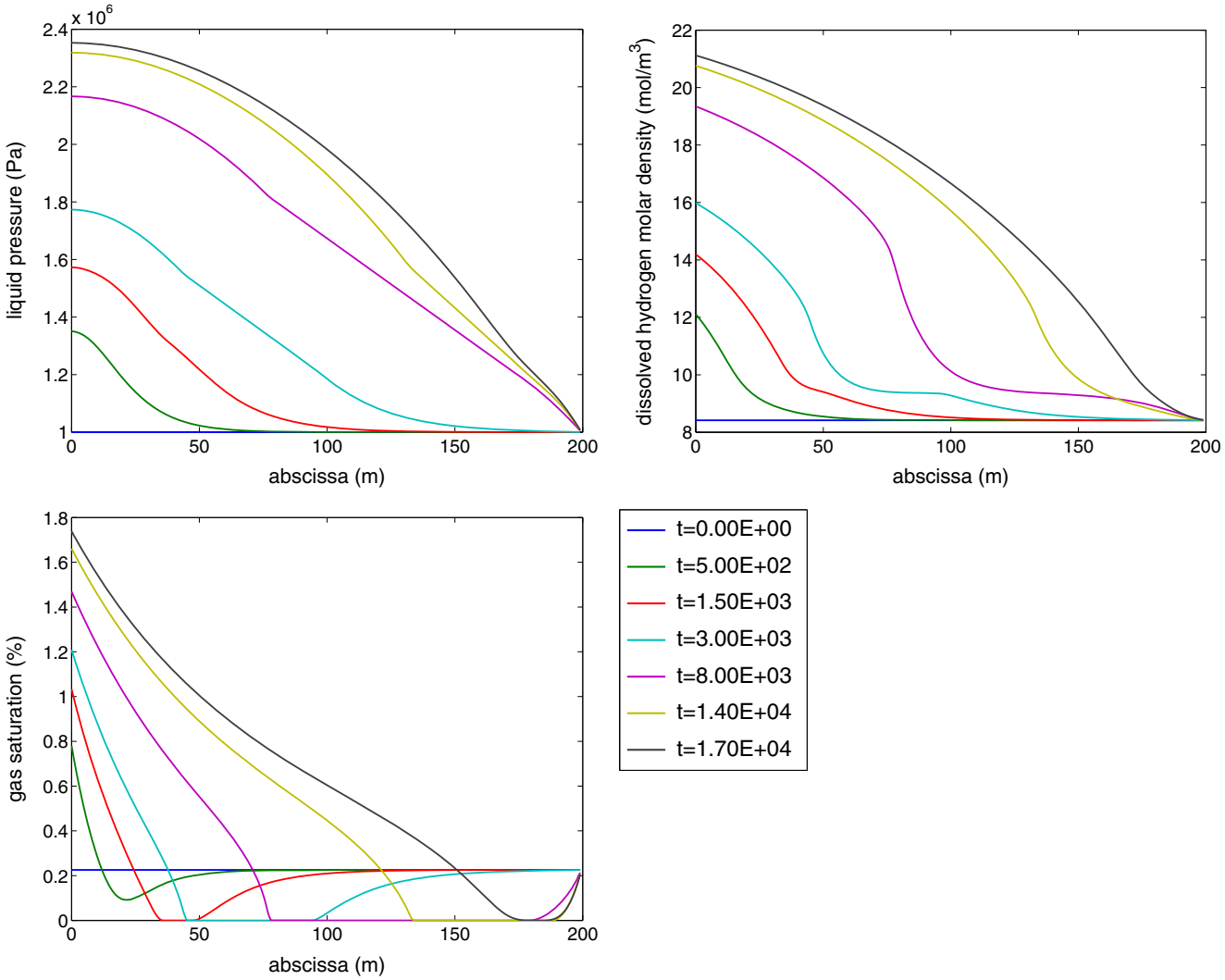

Fig. 6 Test case number 2; $L_x = L_2 = 200$ m. Time evolution, in years, of the dissolved hydrogen molar density $c_{\mathrm{l}}^{\mathrm{h}}$ (*top right*), p_{l} (*top left*), and S_{g} (*bottom*) profiles, during the first period of time

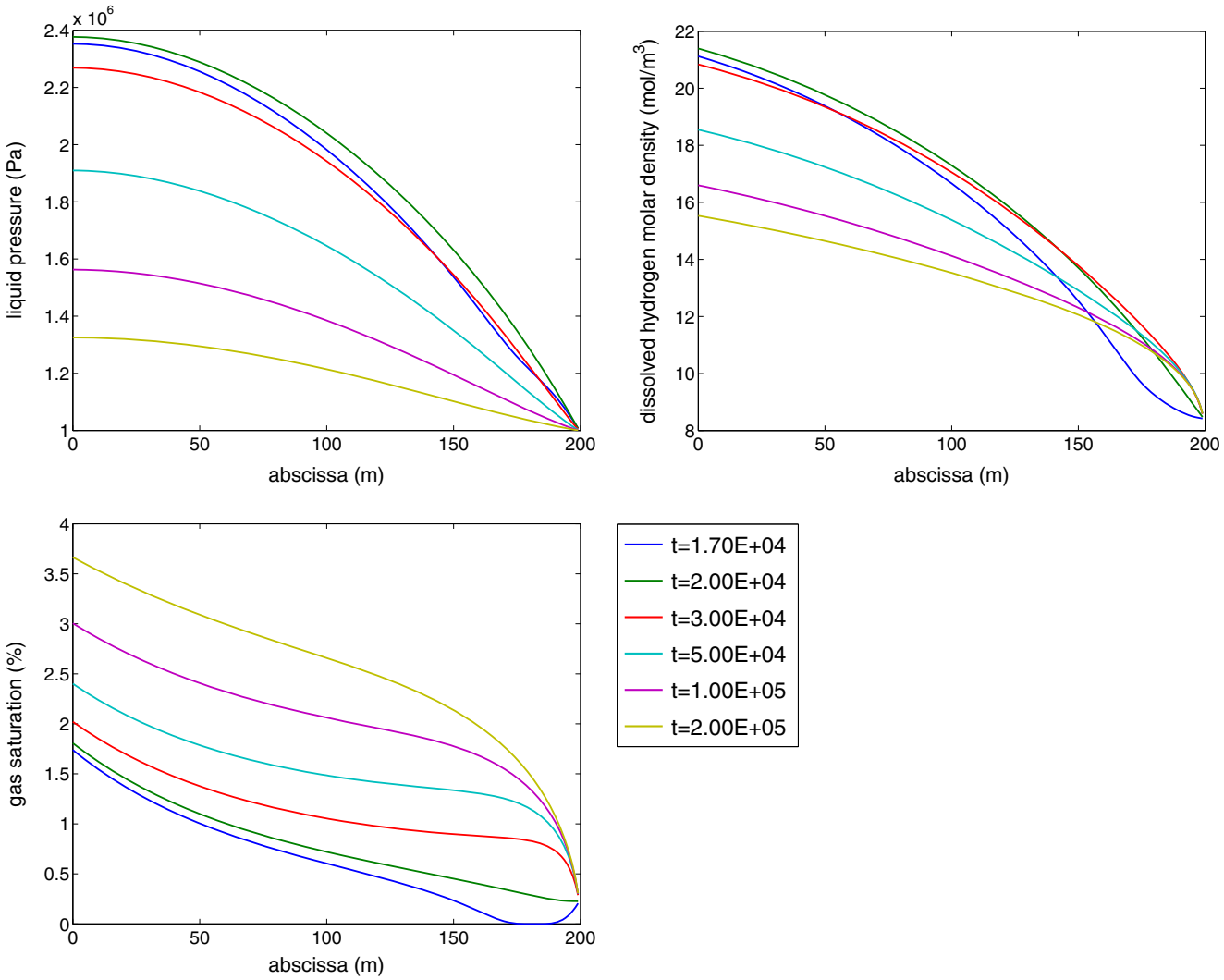

Fig. 7 Test case number 2; $L_x = L_2 = 200$ m. Time evolution, in years, of the dissolved hydrogen molar density c_l^h (*top right*), p_l (*top left*), and S_g (*bottom*) profiles, during the last period of time

4.2 Numerical test number 2

The geometry and the data of this numerical test are given in Fig. 4 and Table 4. The porous medium is homogeneous and the initial conditions are uniform; there is no need for defining two parts of the porous domain, Ω_1 and Ω_2. The parameter L_1 will be considered as null.

In this second test, a constant flux of hydrogen is imposed on the input boundary Γ_{in}, while Dirichlet conditions $p_l = p_{l,out}$ and $p_g = p_{g,out}$ are chosen, on

Table 5 Numerical test case number 3: boundary and initial conditions and domain geometry

Boundary conditions	Other	
Initial condition	Parameter	Value
$\phi^w \cdot \nu = 0$ on Γ_{imp}	L_x	200 m
$\phi^h \cdot \nu = 0$ on Γ_{imp}	L_y	20 m
$\phi^w \cdot \nu = 0$ on Γ_{in}	L_1	20 m
$\phi^h \cdot \nu = \mathcal{Q}^h$ on Γ_{in}	$p_{l,out}$	10^6 Pa
$p_l = p_{l,out}$ on Γ_{out}	$\mathcal{Q}^h$	5.57 mg/m^2/year
$\rho_l^h = 0$ on Γ_{out}		
$p_l(t=0) = p_{l,out}$ on Ω		
$\rho_l^h(t=0) = 0$ on Ω		

ϕ^w and ϕ^h are denoting respectively the water and hydrogen flux

Table 6 Numerical test case number 3: porous medium characteristics

	Porous media	
Parameter	Value on Ω_1	Value on Ω_2
k	10^{-18} m^2	$5 \cdot 10^{-20}$ m^2
Φ	0.3	0.15
P_r	$2 \cdot 10^6$ Pa	$15 \cdot 10^6$ Pa
n	1.54	1.49
$S_{l,res}$	0.01	0.4
$S_{g,res}$	0	0

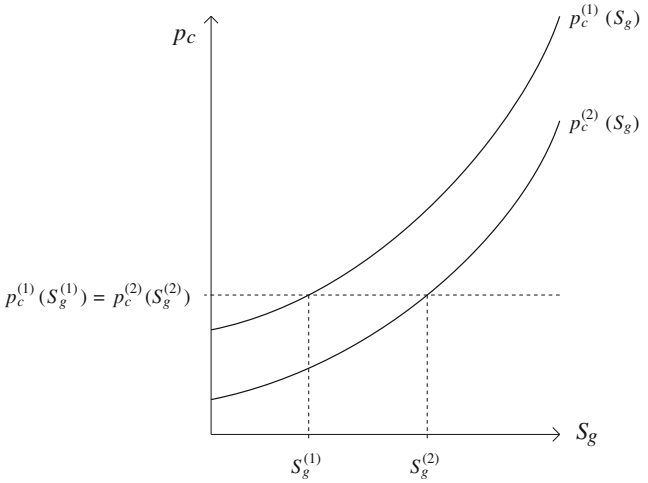

Fig. 8 Saturation discontinuity at the interface of two materials with different capillary pressure curves; test case number 3

Γ_{out}, such that $\rho_{\text{l}}^{\text{h}} > C_{\text{h}} p_{\text{l}}$, in order to keep the gas phase (according to the phase diagram in Fig. 1) present on this part of the boundary. The initial conditions $p_{\text{l}} = p_{\text{l,out}}$ and $\rho_{\text{l}}^{\text{h}} = C_{\text{h}} p_{\text{g,out}}$ are uniform and imply the presence of the gas phase in the whole domain.

The main steps of the corresponding simulation are presented in Figs. 6 and 7 where we show the liquid pressure p_{l}, the dissolved hydrogen molar density c_{l}^{h} (equal to $\rho_{\text{l}}^{\text{h}}/M^{\text{h}}$), and the gas saturation S_{g} profiles, at different times.

At the beginning, up to $t < 1{,}400$ years, the two phases are present in the whole domain (see time $t =$ 500 years in Fig. 6). The permanent injection of hydrogen increases the gas saturation in the vicinity of Γ_{in}. The local gas saturation drop is due to the difference in relative mobilities $\lambda_\alpha(S_\alpha)$ between the two phases: the lower liquid mobility leads to a bigger liquid pressure

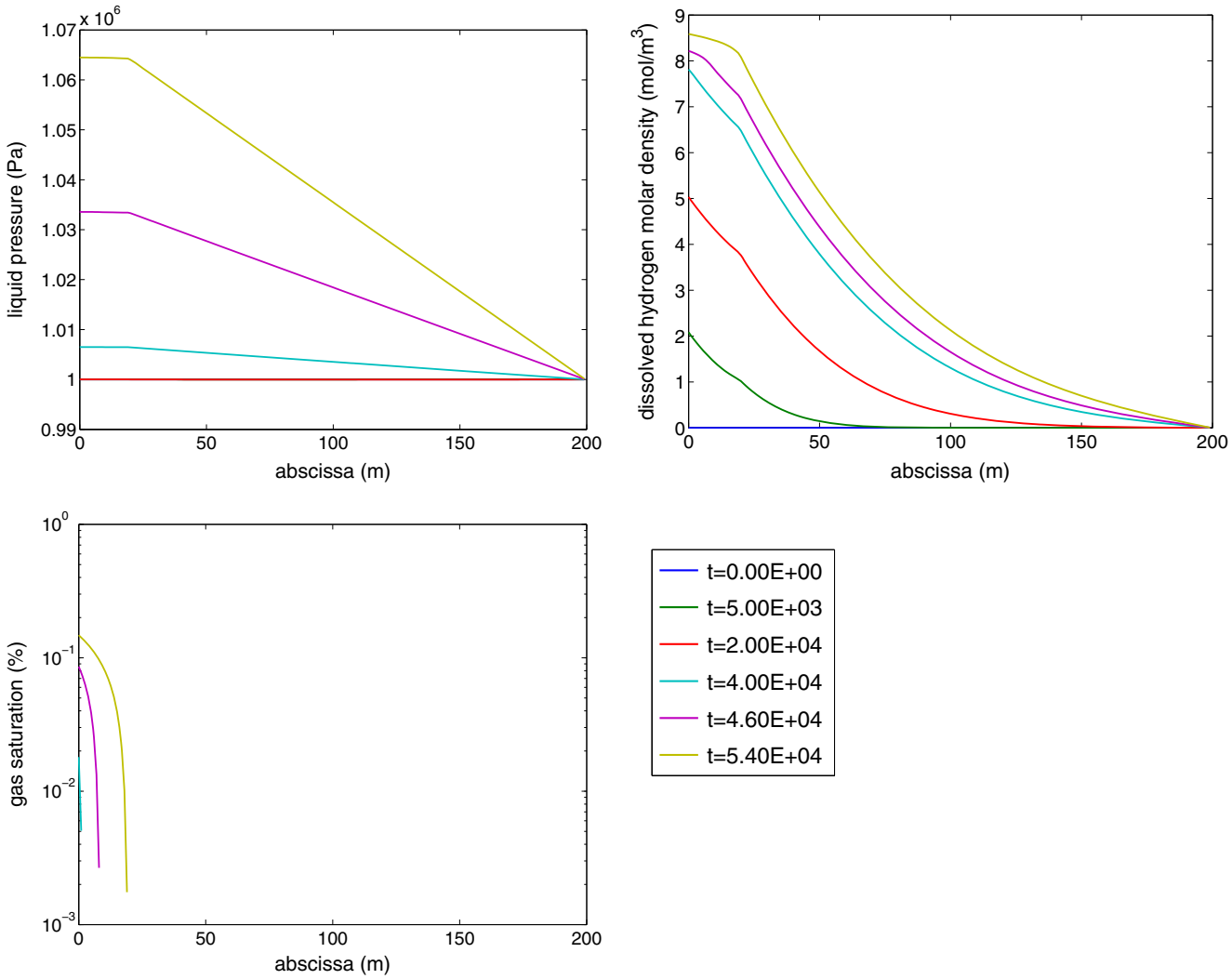

Fig. 9 Test case number 3; $L_x = 200$ m, $L_1 = 20$ m. Time evolution, in years, of the dissolved hydrogen molar density c_{l}^{h} (*top right*), p_{l} (*top left*), and S_{g} (*bottom*) profiles, during the first period of time

increase, compared to the gas pressure increase, which is finally producing a capillary pressure drop (according to definitions (1) and (3), see Fig. 2) and creating a liquid saturated zone. At time $t = 1{,}400$ years, the gas phase starts to disappear in some region of the porous domain (see time $t = 1{,}500$ years, in Fig. 7).

Then, a saturated liquid region ($S_g = 0$) will exist until time $t = 17{,}000$ years (see Fig. 6), and during this period of time, the saturated region is pushed by the injected hydrogen, from Γ_{in} to Γ_{out}.

After the time $t = 17{,}000$ years, due to the Dirichlet conditions imposed on Γ_{out}, the liquid saturated region disappears and all together the phases' pressure and the gas saturation are growing in the whole domain (see the time $t = 20{,}000$ years in Fig. 7).

Finally, the liquid pressure reaches its maximum at time $t = 20{,}000$ years and then decreases in the whole domain (see Fig. 7). This is caused, like in the numerical test case number 1, by the evolution of the system towards a stationary state which is characterized by a zero water component flow.

4.3 Numerical test number 3

The geometry and the data of this numerical test are given in Fig. 4 and Tables 5 and 6. Like in the numerical test number 2, a constant flux of hydrogen is imposed on the input boundary, Γ_{in}, while Dirichlet conditions $p_l = p_{l,out}$ and $\rho_l^h = 0$ are given on Γ_{out}, in order to have only the liquid phase on this part of the boundary. The initial conditions, $p_l = p_{l,out}$ and $\rho_l^h = 0$, are uniform on all the domain and correspond to a porous domain initially saturated with pure water. Contrary to the two

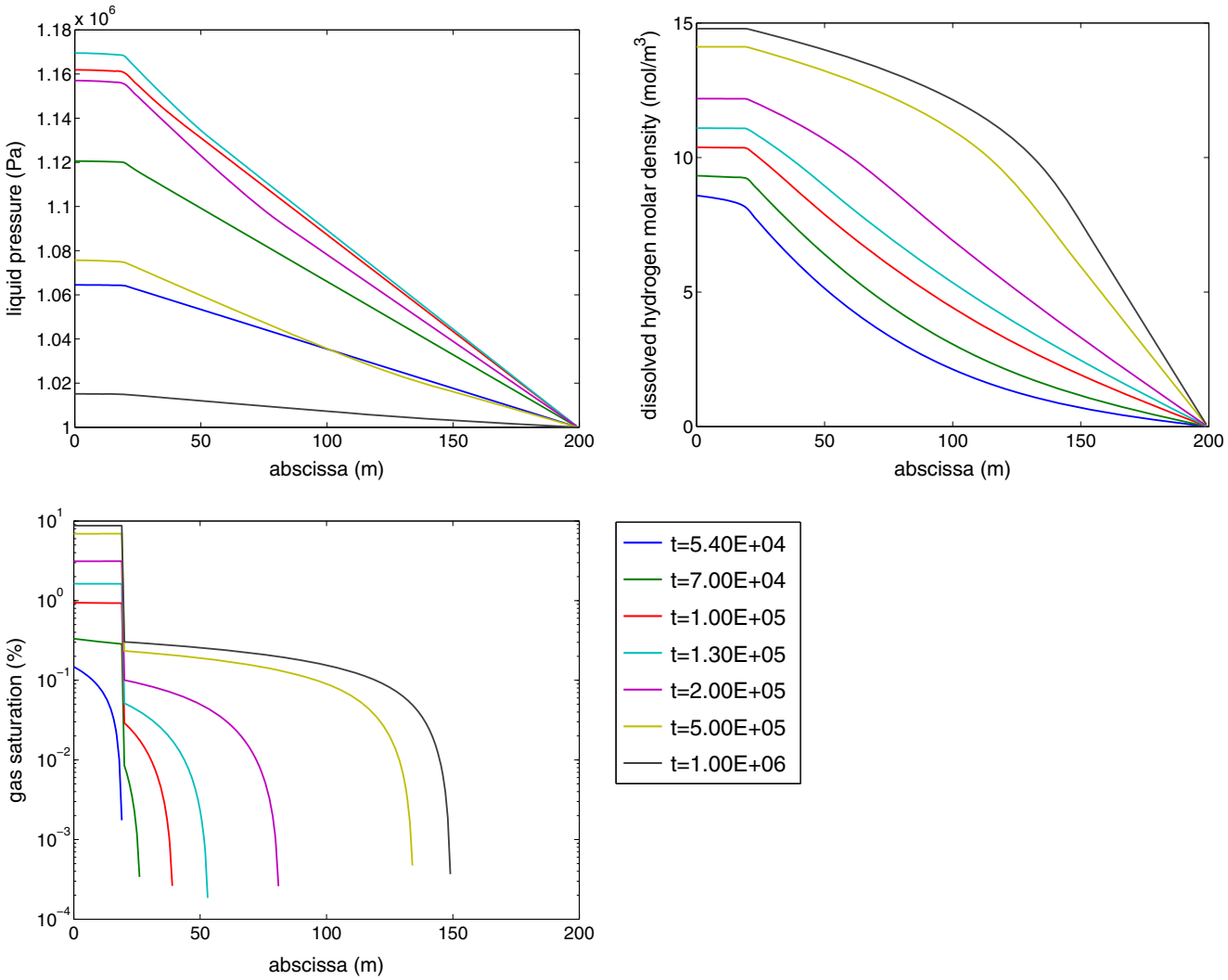

Fig. 10 Test case number 3; $L_x = 200$ m, $L_1 = 20$ m. Time evolution, in years, of the dissolved hydrogen molar density c_l^h (*top right*), p_l (*top left*), and S_g (*bottom*) profiles, during the last period of time

first numerical tests, the porous domain is nonhomogeneous and there are two different porous subdomains Ω_1 and Ω_2; $L_x = 200$ m, $L_1 = 20$ m, and $L_2 = 180$ m.

The simulation time of this test case is $T = 10^6$ years, the discretization space mesh is 1 m, and the time step is 10^2 years at the beginning and grows up to $2 \cdot 10^4$ years in the end of the simulation (see Table 2).

Figures 9 and 10 represent the liquid pressure p_l, the dissolved hydrogen molar density (equal to ρ_l^h / M^h), and the gas saturation S_g profiles at different times.

The main difference from the previous simulations (which were in a homogeneous porous domain) is the gas saturation discontinuity (Fig. 8), staying on the porous domain interface $x = 20$ m. Due to the height of this saturation jump , we had to use a logarithm scale for presenting the gas saturation S_g profiles, but as a consequence, although all the S_g curves go to zero, this cannot be seen with a logarithmic scale in Figs. 9 and 10.

There are four main steps:

- From 0 to $3.8 \cdot 10^4$ years, the increase of both the gas saturation and the liquid pressure is small and slow in the whole domain and hard to see on the figures, while the hydrogen injection on the left side Γ_{in} of the domain increases notably the hydrogen density level.
- From $3.8 \cdot 10^4$ to $5.4 \cdot 10^4$ years, both the liquid pressure and the hydrogen density are increasing in the whole domain. The gas starts to expand from the left side of the domain Γ_{in}. The saturation front moved towards the porous media discontinuity, at $x = 20$ m, which is reached at $t = 5.4 \cdot 10^4$ years; see Fig. 9.
- From $5.4 \cdot 10^4$ to $1.3 \cdot 10^5$ years, see Fig. 10, the saturation front has crossed the medium discontinuity at $x = 20$ m, and from now, all the saturation profiles will have a discontinuity at $x = 20$ m.
- From $1.3 \cdot 10^5$ to 10^6 years, see Fig. 10, both the hydrogen density and the gas saturation keep growing while the liquid pressure decreases towards zero on the entire domain. The gas saturation front keeps moving to the right, pushed by the injected gas, up to $x \approx 150$ m at 10^6 years.

Until the saturation front reaches the interface between the two porous media, for ($t = 5.4 \cdot 10^4$ years), appearance and evolution of both the gas phase and the unsaturated zone are identical to what was happening in test number 1 (with a homogeneous porous domain) during the period of gas injection: the dissolved hydrogen is accumulating at the entrance until the liquid phase becomes saturated, at time $t > 3.8 \cdot 10^4$ years, letting the gas phase to appear.

When the saturation front crosses the interface between the two porous subdomains (at $x = 20$ m and $t = 5.4 \cdot 10^4$ years), the gas saturation is strictly positive on both sides of this interface and the capillary pressure curves is different on each side (see Table 6). The capillary pressure continuity at the interface imposes to $p_c^{(1)}$ the capillary pressure in Ω_1 and to $p_c^{(2)}$ the capillary pressure in Ω_2, to be equal on this interface. Then, $p_c^{(1)} = p_c^{(2)}$ is satisfied only if there are two different saturations, on each interface side $S_g^{(1)}$ and $S_g^{(2)}$: $p_c^{(1)}(S_g^{(1)}) = p_c^{(2)}(S_g^{(2)})$, see Fig. 8.

In the same way as in the numerical test number 1, the system tends to a stationary state.

4.4 Numerical test number 4

This last numerical test is different from all the precedent ones. It intends to be a simplified representation of what happens when an unsaturated porous block is placed within a water-saturated porous structure. The challenge is then how the mechanical balance will be restored in a homogeneous porous domain, which was initially out of equilibrium, i.e., with a jump in the initial phase pressures?

The initial liquid pressure is the same in the entire porous domain; Ω, $p_{l,1} = p_{l,2}$, and in the subdomain Ω_1, the initial condition, $p_{l,1} = p_{g,1}$, in Table 7 correspond to a liquid fully saturated state with a hydrogen concentration reaching the gas appearance concentration threshold ($p_g = p_l$ and $\rho_l^h = C_h p_g$, Fig. 1). In the subdomain Ω_2, the initial condition ($p_{l,2} \neq p_{g,2}$ and $p_{g,2} \neq p_{g,1}$) corresponds to a nonsaturated state (see Table 7).

Table 7 Data of the numerical test number 4: boundary and initial conditions and domain geometry

Boundary conditions	Porous medium	
Initial condition	Parameter	Value
$\phi^w \cdot \nu = 0$ on $\partial\Omega$	k	10^{-18} m^2
$\phi^h \cdot \nu = 0$ on $\partial\Omega$	Φ	0.3
$p_l(t=0) = p_{l,1}$ on Ω_1	P_r	$2 \cdot 10^6$ Pa
$\rho_l^h(t=0) = C_h p_{g,1}$ on Ω_1	n	1.54
$p_l(t=0) = p_{l,2}$ on Ω_2	$S_{l,res}$	0.01
$\rho_l^h(t=0) = C_h p_{g,2}$ on Ω_2	$S_{g,res}$	0
$p_{l,1} = 10^6$ Pa	Other	
$p_{g,1} = 10^6$ Pa	Parameter	Value
$p_{l,2} = 10^6$ Pa	L_x	1 m
$p_{g,2} = 2.5 \cdot 10^6$ Pa	L_y	0.1 m
	L_1	0.5 m

The porous medium domain Ω is homogeneous. All the porous medium parameters are the same in the two subdomains Ω_1 and Ω_2; ϕ^w and ϕ^h are denoting respectively the water and hydrogen flux

The porous block initial state is said out of equilibrium since if this initial state was in equilibrium, in the two subdomains Ω_1 and Ω_2, the local mechanical balance would have made the pressures, of both the liquid and the gas phase, continuous in the entire domain Ω.

For simplicity, we assume that the porous medium domain Ω is homogeneous and all the porous medium characteristics are the same in the two subdomains Ω_1 and Ω_2, and corresponding to concrete. The system is then expected to evolve from this initial out of equilibrium state towards a stationary state.

We should notice that, in order to see the final stationary state appearing, in a reasonable period of time, we have shortened the domain Ω ($L_x = 1$ m), taken the porous media characteristics, and set the final time of this simulation T_{fin} at $T_{\text{fin}} = 10^6$ s ≈ 11.6 days. The complete set of data of this test case is given in Table 7.

The space discretization step was taken constant equal to $2 \cdot 10^{-3}$ m and the time step was variable, going from 0.33 s in the beginning of the simulation to $16.7 \cdot 10^3$ s at the end of the simulation (see Table 2). Figures 11 and 12 represent the liquid pressure p_l, the dissolved hydrogen molar concentration c_l^h, and the gas saturation S_g profiles at different times.

There are essentially two steps:

– For $0 < t < 1.92 \cdot 10^5$ s (see Fig. 11), the initial gas saturation jump moves from $x = 0.5$ m, at $t = 0$, and reaches Γ_{in}, the left domain boundary, at $t = 1.92 \cdot 10^5$ s. During this movement, the saturation jump height (initially ≈ 0.16) decreases, until ap-

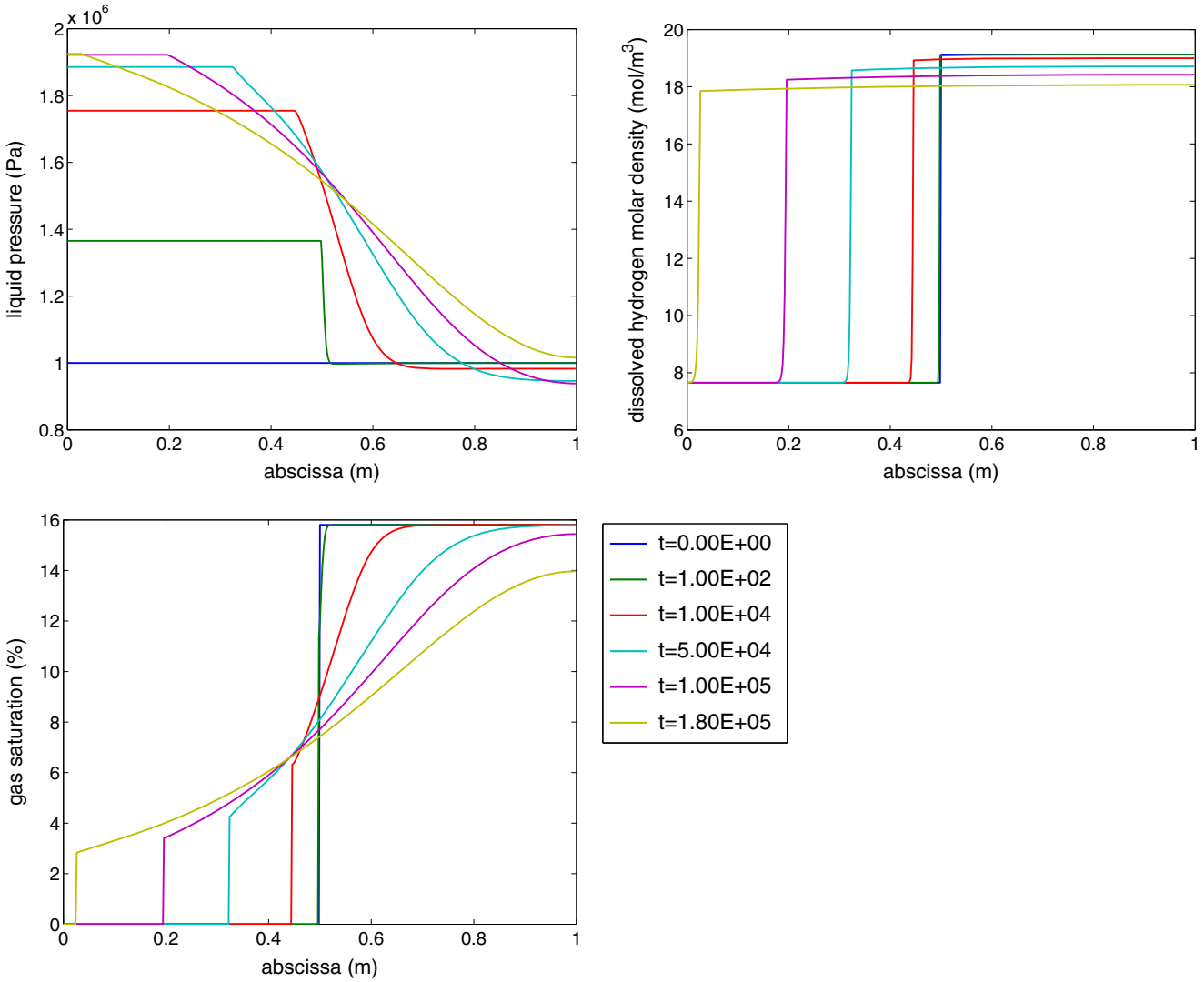

Fig. 11 Numerical test case number 4, $L_x = 1$ m, $L_1 = 0.5$ m: time evolution, in seconds, of the dissolved hydrogen molar density c_l^h (*top right*), p_l (*top left*), and S_g (*bottom*) profiles, during the first period of time

proximately 0.03, when it reaches the left boundary Γ_{in}. In front of this discontinuity, there is a liquid saturated zone, $S_g = 0$, and in this zone, both the liquid pressure and the hydrogen density are spatially uniform (see Fig. 11, top). But, while the hydrogen density remains constant and equal to its initial value, the liquid pressure becomes immediately continuous and starts growing quickly (for instance, $p_l(t = 10^3 \text{ s}) \approx 1.6 \cdot 10^6$ Pa) and then more slowly until $t = 1.3 \cdot 10^5$ s, when it starts to slightly decrease.

In Fig. 11, located on the gas saturation discontinuity, there are both a high contrast in the dissolved hydrogen concentration (this concentration stays however continuous, but with a strong gradient, as seen in the top right of Fig. 11) and a discontinuity in the liquid pressure gradient (see the top left of Fig. 11).

– For $1.92 \cdot 10^5$ s $< t < 10^6$ $s = T_{fin}$ (see Fig. 12), all the entire domain is now unsaturated ($S_g > 0$). The liquid pressure, the hydrogen density, and the gas saturation profiles are all strictly monotonous and continuous, going towards a spatially uniform distribution, corresponding to the stationary state (see Fig. 12).

As expected, the system initially out of equilibrium (discontinuity of the gas pressure) comes back immediately to equilibrium (the gas pressure is continuous) and evolves towards a uniform stationary state (due to the no mass inflow and outflow boundary conditions). Although the liquid pressure and the dissolved

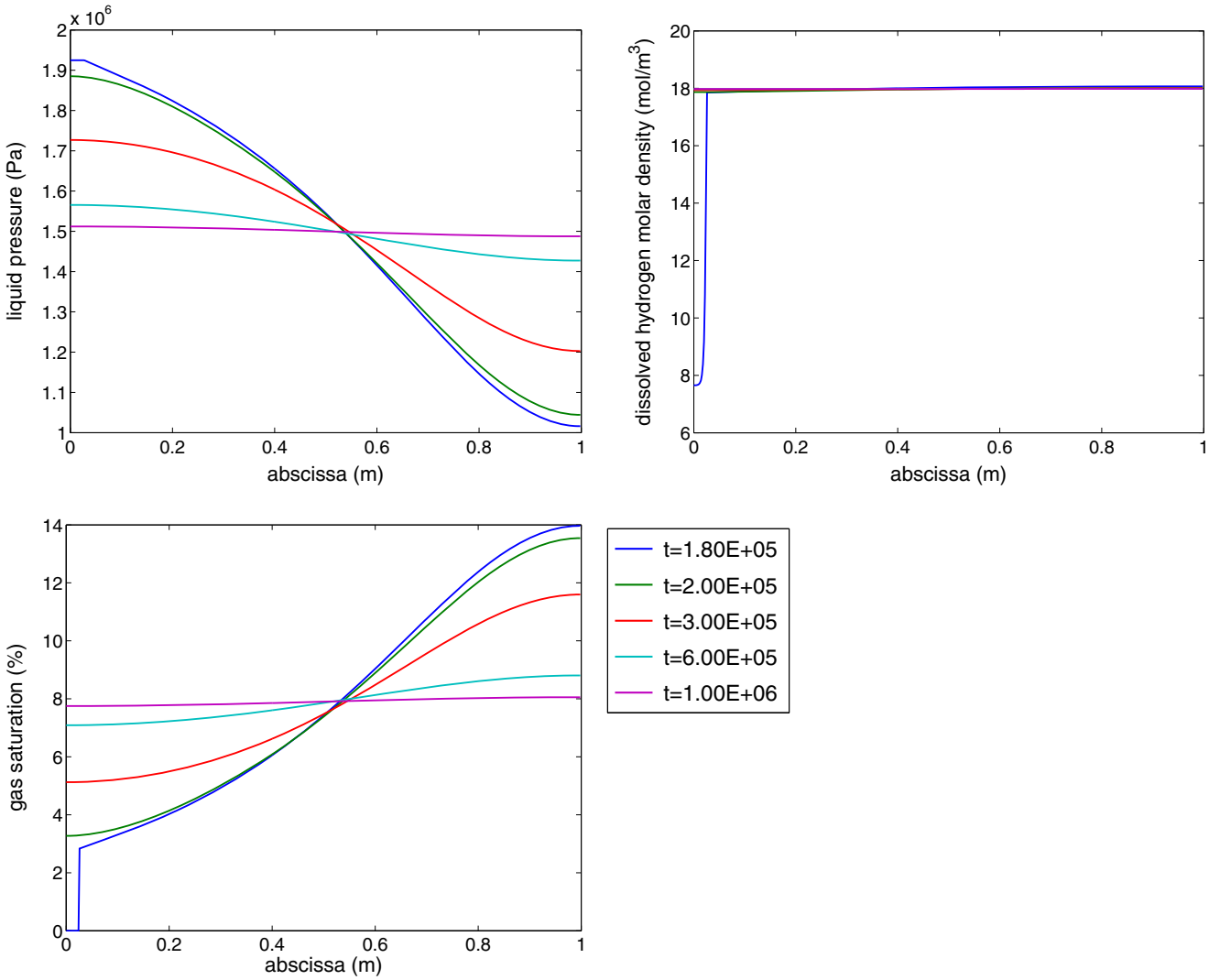

Fig. 12 Numerical test case number 4, $L_x = 1$ m, $L_1 = 0.5$ m: time evolution, in seconds, of the dissolved hydrogen molar density c_l^h (*top right*), p_l (*top left*), and S_g (*bottom*) profiles, during the last period of time

hydrogen density are immediately again continuous for $t > 0$, the hydrogen density still has a locally very strong gradient until $t = 1.92 \cdot 10^5$ s.

At first, and at the very beginning ($\approx 10^2$ s), see top left of Fig. 11, only the liquid pressure evolves in the liquid saturated zone. Due to the gas pressure in the unsaturated zone which is higher than in the liquid saturated zone ($S_g = 0$, $p_g = 2.5$ MPa $> p_l = 1$ MPa, for the initial state in Table 7), and due to the no flow condition imposed on Γ_{in}, the liquid in the saturated zone is compressed by the gas from the unsaturated zone. Then, a liquid gradient pressure appears around the saturation front and makes the liquid to flow from the liquid saturated zone towards the unsaturated one and then makes the gas saturation front to move in the opposite direction.

The very strong hydrogen density gradient (until $t = 1.92 \cdot 10^5$ s), located on the saturation front, is due to the competition between the diffusion and the convective flux of the dissolved hydrogen around the saturation front: the water flow convecting the dissolved hydrogen, from left to right, cancels the smoothing effect of the gas diffusion propagation in the opposite direction. On the one hand, the diffusion is supposed to reduce the hydrogen concentration contrast, by creating a flux going from strong concentrations (in the unsaturated zone) towards the low concentrations (in the liquid saturated zone), and on the other hand, the flow of the liquid phase goes in the opposite direction (left to right, from $S_g = 0$ to $S_g > 0$). Once the disequilibrium has disappeared, the system tends to reach a uniform stationary state determined by the mass conservation of each component present in the initial state (the system is isolated, with no flow on any of the boundaries).

5 Concluding remarks

From balance equations, constitutive relations and equations of state, assuming thermodynamical equilibrium, we have derived a model for describing two-phase flows in both saturated and unsaturated porous media, including diffusion of components in phases and capillary effects.

In the second part, we have presented a group of numerical test cases synthesizing the main challenges concerning the gas migration in a deep geological repository. These numerical simulations are based on simplified but typical situations in underground nuclear waste management; they show evidence of the model's ability to describe the gas (hydrogen) migration and to treat the difficult problem of correctly following the saturated and unsaturated regions created by the gas generation. The optimal selection of primary variables depends, in general, on the characteristics of the particular problem being simulated, and in some circumstances, it may have a large effect on the conditioning of the Jacobian matrix and hence on the number of Newton iterations and the number of iterations required to solve the Jacobian system. Moreover, the evaluation of secondary variables may require further solving of nonlinear algebraic equations and then may have a large impact on efficiency of the chosen set of primary variables. For instance, the formulation in Section 3.1, based on the total hydrogen density, is better adapted to problems with little capillary effects, but the secondary variable such as the saturation is given implicitly and has to be calculated by Newton iterations at every point.

In highly heterogeneous media, it is also important to choose the primary variables which are continuous through material interfaces (like the phase pressure and dissolved hydrogen mass ρ_l^h as in Section 3.2), than variables like saturations or total hydrogen mass which are discontinuous through the interface.

Although the formulation based on total hydrogen mass is more suitable when the capillary effects are negligible, it is shown in the numerical tests presented herein that the primary variables chosen in Section 3.2 can efficiently treat situations of gas appearance/disappearance, in the presence of heterogeneities, similar to situations appearing in simulating gas migration in deep geological repository for radioactive waste.

Acknowledgements This work was partially supported by the GNR MoMaS (PACEN/CNRS, ANDRA, BRGM, CEA, EDF, IRSN). Most of the work on this paper was done when Mladen Jurak was visiting, at Université Lyon 1, the CNRS-UMR 5208 ICJ.

References

1. Abadpour A., Panfilov M.: Method of negative saturations for two-phase compositional flow with oversaturated zones. Transp. Porous Media **79**, 197–214 (2009)
2. Allen III, M.B.: Numerical modelling of multiphase flow in porous media. Adv. Water Resour. **8**, 162–187 (1985)
3. Andra, D.: http://www.andra.fr/international/pages/en/dossier-2005-1636.html (2005). Accessed 25 October 2012
4. Angelini, O., Chavant, C., Chénier, E., Eymard, R., Granet, S.: Finite volume approximation of a diffusion–dissolution model and application to nuclear waste storage. Math. Comput. Simul. **81**, 2001–2017 (2011)
5. Bear, J.: Dynamics of Fluids in Porous Media. Elsevier, New York (1979)
6. Bear, J., Bachmat, Y.: Introduction to Modeling of Transport Phenomena in Porous Media. Kluwer, Dordrecht (1991)
7. Bear, J., Bensabat, J., Nir, A.: Heat and mass transfer in unsaturated porous media at a hot boundary: I. One-

dimensional analytical model. Transp. Porous Media **6**, 281–298 (1991)
8. Bonina, B., Colina, M., Dutfoy, A.: Pressure building during the early stages of gas production in a radioactive waste repository. J. Nucl. Mater. **281**(1), 1–14 (2000)
9. Bourgeat, A., Jurak, M., Smaï, F.: Two partially miscible flow and transport modeling in porous media; application to gas migration in a nuclear waste repository. Comput. Geosci. **13**(1), 29–42 (2009)
10. Brooks, R.J., Corey, A.T.: Properties of porous media affecting fluid flow. In: Proc. Am. Soc. Civil Eng. (IR2); J. Irrig. Drain. Div. **92**, 61–88 (1966)
11. CEA: Cast3m, http://www-cast3m.cea.fr (2003). Accessed 25 January 2012
12. Chavent, G., Jaffré, J.: Mathematical Models and Finite Elements for Reservoir Simulation. North-Holland, Amsterdam (1986)
13. Class, H., Helmig, R., Bastian, P.: Numerical simulation of non-isothermal multiphase multicomponent processes in porous media 1. An efficient solution technique. Adv. Water Resour. **25**, 533–550 (2002)
14. Class, H., Dahle, H.K., Helmig, R. (eds.): Special issue: numerical models for carbon-dioxide storage in geological formations. Comput. Geosci. **13**(4), 405–509 (2009)
15. Delshad, M., Thomas, S.G., Wheeler, M.F.: Parallel numerical reservoir simulations of non-isothermal compositional flow and chemistry. SPE-118847-PP (2009)
16. Facchinei, F., Pang, J.S.: Finite Dimensional Variational Inequalities and Complementarity Problems. Springer, New York (2003)
17. Firoozabadi, A.: Thermodynamics of Hydrocarbon Reservoirs. McGraw-Hill, New York (1999)
18. FORGE project: http://www.forgeproject.org (2012). Accessed 25 October 2012
19. Draft report on definition of benchmark studies on repository-scale numerical simulations of gas migration, FORGE Reports, D1.1. http://www.bgs.ac.uk/forge/docs/reports/D1.1.pdf (2009). Accessed 25 October 2012
20. Progress report on benchmark studies on repository-scale numerical simulations of gas migration, FORGE Work Packages 2 Reports, D1.3. http://www.bgs.ac.uk/forge/docs/reports/D1.3.pdf (2010). Accessed 25 October 2012
21. Forsytha, P.A., Unger, A.J.A., Sudicky, E.A.: Nonlinear iteration methods for nonequilibrium multiphase subsurface flow. Adv. Water Resour. **21**, 433–449 (1998)
22. Jaffré, J., Sboui, A.: Henry's law and gas phase disappearance. Transp. Porous Media **82**, 521–526 (2010)
23. Jin, Y., Jury, W.A.: Characterizing the dependence of gas diffusion coefficient on soil properties. Soil Sci. Soc. Am. J. **60**, 66–71 (1996)
24. Knabner, P., Marchand, E., Müller, T.: Fully coupled generalised hybrid-mixed finite element approximation of two-phases two-components flow in porous media. Part II: numerical scheme and numerical results. Comput. Geosc. **16**, 691–708 (2012)
25. Kräutle, S.: The semismooth Newton method for multicomponent reactive transport with minerals. Adv. Water Res. **34**, 137–151 (2011)
26. Lauser, A., Hager, C., Helmig, R., Wohlmuth, B.: A new approach for phase transitions in miscible multi-phase flow in porous media. Adv. Water Resour. **34**, 957–966 (2011)
27. Marle, C.M.: Multiphase Flow in Porous Media. Édition Technip, Paris (1981)
28. Mualem, Y.: A new model for predicting the hydraulic conductivity of unsaturated porous media. Water Resour. Res. **12**(3), 513–522 (1976)
29. NAGRA: Demonstration of disposal feasibility for spent fuel, vitrified waste and long-lived intermediate-level waste. Technical report NTB 02-05 (2002)
30. NDA: Geological disposal: steps towards implementation (2010)
31. NEA: Engineered Barrier Systems (EBS): design requirements and constraints, workshop proceedings, Turku, Finland, 26–29 August 2003. In co-operation with the European Commission and hosted by Posiva Oy, OECD/Nuclear Energy Agency, Paris, France (2004)
32. Oladyshkin, S., Panfilov, M.: Hydrogen penetration in water through porous medium: application to a radioactive waste storage site. Environ. Earth Sci. **64**(4), 989–999 (2011). doi:10.1007/s12665-011-0916-0
33. Olivella, S., Alonso, E.E.: Gas flow through clay barriers. Geotechnique **58**(3), 157–176 (2008)
34. Safety of Geological Disposal of High-level and Long-lived Radioactive Waste in France, OECD 2006, NEA No. 6178. http://www.oecd-nea.org/rwm/reports/2006/nea6178-argile.pdf. Accessed 25 October 2012
35. Olivella, S., Carrera, J., Gens, A., Alonso, E.E.: Non-isothermal multiphase flow of brine and gas through saline media. Transp. Porous Media **15**, 271–293 (1994).
36. ONDRAF/NIRAS: Safir 2. Safety Assessment and Feasibility Interim Report 2, NIROND 2001-06E, Brussels, Belgium (2001)
37. PAMINA project: http://www.ip-pamina.eu (2011). Accessed 25 January 2012
38. Panday, S., Forsyth, P.A., Falta, R.W., Wu, Y.-S., Huyakorn, P.S.: Considerations for robust compositional simulations of subsurface nonaqueous phase liquid contamination and remediation. Water Resour. Res. **31**, 1273–1289 (1995)
39. Peaceman, D.W.: Fundamentals of Numerical Reservoir Simulation. Elsevier, Amsterdam (1977)
40. Pruess, K., Oldenburg, C., Moridis, G.: Tough2 user's guide, version 2.0. Lawrence Berkeley National Laboratory, Berkeley (1999)
41. Talandier, J.: Synthèse du benchmark couplex-gaz. In: Journées Scientifiques du GNR MoMaS, Lyon, 4–5 Septembre 2008. http://momas.univ-lyon1.fr/presentations/couplex_lyon2008_andra.ppt. Accessed 25 January 2012
42. Van Genuchten, M.: A closed form equation for predicting the hydraulic conductivity of unsaturated soils. Soil Sci. Soc. Am. J. **44**, 892–898 (1980)
43. Wua, Y.-S., Forsyth, P.A.: On the selection of primary variables in numerical formulation for modeling multiphase flow in porous media. J. Contam. Hydrol. **48**, 277–304 (2001)
44. Hintermuller, M., Ito, K., Kunisch, K.: The primal-dual active set strategy as a semismooth Newton method. SIAM J. Optim. **13**, 865–888 (2002)